AD-A141 050 INTRINSIC MECHANISMS OF MULTI-LAYER CERAMIC CAPACITOR FAILURE(U) VIRGINIA POLYTECHNIC INST AND STATE UNIV BLACKSBURG L C BURTON APR 84 N00014-83-K-0168 1/1

UNCLASSIFIED F/G 9/1 NL

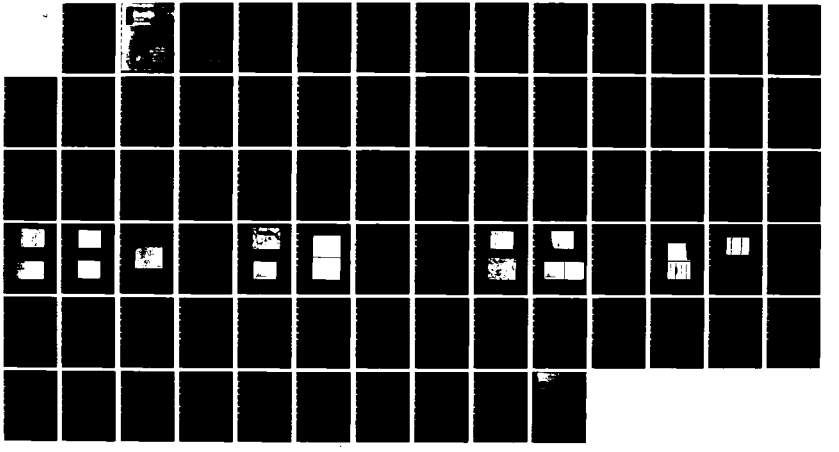

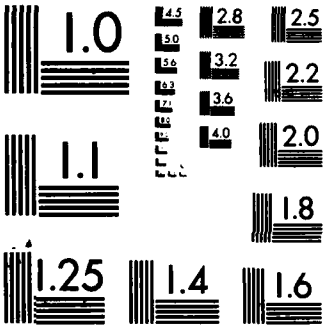

COLLEGE OF ENGINEERING

CERAMIC CAPACITOR FAILURE

ANNUAL REPORT

Time Period: 3/15/83- [illegible]

ONR Contract No. N0001[illegible]

Principal Investigator: [illegible]

April, 1984

[illegible]tments of Electrical Engineering and [illegible]

VIRGINIA POLYTECHNIC INSTITUTE AND STATE UNIVERSITY

BLACKSBURG, VIRGINIA

INTRINSIC MECHANISMS OF MULTI-LAYER CERAMIC CAPACITOR FAILURE

ANNUAL REPORT

Time Period: 3/15/83-3/14/84

ONR Contract No. N00014-83-K-0168

Principal Investigator: L. C. Burton

April, 1984

Departments of Electrical Engineering and Materials Engineering
Virginia Polytechnic Institute and State University
Blacksburg, VA 24061

TABLE OF CONTENTS

SUMMARY OF RESULTS

1. DC leakage currents for Z5U and X7R MLC capacitors follow a near 3/2 power voltage dependence when new; this generally transforms into a higher power dependence (V^2 being common) at voltages greater than a few volts, with ohmic behavior at lower voltages, as degradation proceeds; with further degradation the characteristic becomes ohmic over the entire voltage range;

2. The 3/2 power and square law voltage behavior can be modelled after space charge limited currents; the 3/2 case can be attributed to electron emission from cathode points and protuberances, the square law case to emission from planar electrode regions;

3. Thermoelectric voltages and space charge limited currents verify that the electron is the main charge carrier (transported by small polaron hopping);

4. Carrier concentrations (n) and drift mobilities (μ) have been deduced from thermoelectric measurements on new and reduced non-electroded X7R ceramic chips; n and μ both increase substantially with reduction, with mobility dominating the thermal activation energy (donors are $\approx$ completely ionized);

5. For X7R capacitors, thermal activation energies decrease from about 1.3eV to zero as resistivity (at 125°C) decreases from $\sim 10^{13}$ Ω-cm to $\sim 10^{5}$ Ω-cm or less;

6. Schottky or Poole-Frenkel currents were not identified;

7. Estimates of mobility, trap concentration and trap energy were made from quadratic space charge current characteristics;

8. Electrode protuberances spanning a large range of sizes were seen on cross sectioned devices; these are correlated to the $V^{3/2}$ dependence of leakage current;

9. Symmetric color gradients between electrodes were seen in degraded devices. These are probably due to oxygen gradients;

10. Compositional gradients could not be detected using Auger electron spectroscopy. This means that the gradients are less than ~0.1 atomic percent, which can still have a large effect on electrical properties;

11. Regions of Zn and Cd segregation were detected on polished devices by means of energy dispersive x-ray analysis;

12. Significant changes in frequency dependence of impedance parameters for degraded devices were not seen, leading to some conclusions about grain boundary space charge layers in these devices.

1. INTRODUCTION

1.1 Objectives and Approaches of Study

The major objective of this research is to obtain an improved understanding of degradation mechanisms of MLC capacitors. This is being approached from several directions:

a) Capacitors (mainly Z5U and X7R types) that are new or in various degrees of degradation (as judged by insulation resistance) have been cross sectioned for SEM and optical examination, and for compositional measurements using energy dispersive x-ray analysis (EDAX), Auger electron spectroscopy (AES), and electron beam microprobe.

b) Electrical measurements on similar devices include current-voltage, current-temperature and impedance-frequency.

c) Thermoelectric measurements have been made on non-electroded X7R chips in order to separate the carrier concentration from the drift mobility, and to observe their change following reduction of the ceramic.

1.2 Degradation Mechanisms

MLC capacitor failure modes were reviewed at the National Academy of Sciences Workshop held in March 1982.[1] Extrinsic and intrinsic mechanisms were discussed, with extrinsic ones receiving the major share of attention due to their more immediate relevancy to fabrication steps and screening.

Extrinsic mechanisms are due for the most part to defective or non-optimized processing, to damage by user, to environmental reactions, etc. and are responsible for most of the infant mortalities.

Intrinsic mechanisms are due to the inherent chemistry and physics of the device, and not to faulty manufacture. Mechanisms included here are ionic migration (including vacancies), electrode-ceramic reaction or cross diffusion, segregation or phase separation, metal nodule formation, etc. Many of these mechanisms are of a longer term nature than the extrinsic ones. However, for high reliability devices with desired long life, they are just as important and will become even more so in the future, as mechanical flaws are reduced by improved processing, and as dielectric layers become thinner.

Extrinsic and intrinsic mechanisms can result in failure independently, or can be strongly coupled. Examples of independent failures are lead separation (extrinsic) and extensive $O^{=}$ migration (intrinsic). These are coupled, for example, when electric field is enhanced at an electrode protuberance, which accelerates ionic migration, leading to failure. This type of extrinsic mechanical flaw would not be seen in screening, and would not be a problem if not coupled to an intrinsic mechanism. Such a case is discussed in greater detail below.

1.3 Leakage Current Types

The leakage current is the single most important capacitor parameter that we wish to understand. Some of our measurements related to leakage currents were submitted to the Electronic Components Conference (New Orleans, May 1984). A copy of that paper is attached in Appendix II. Our major findings are discussed below — Appendix II contains additional details.

In MLC capacitors, the dominant charge carrier and its mode of transport have not been conclusively identified. Leakage currents have been attributed to Poole-Frenkel emission[2] and to oxygen vacancy diffusion[3,4] (through its 1.19eV activation energy).

More numerous studies have been reported for $BaTiO_3$ single crystal[5-8] and ceramic[9-14] materials. For the ceramic, electron conduction seems predominant,[9,10] with conduction strongly effected by impurities.[11,12] Space large limited currents (SCLC)[5,6,12,13] and Schottky currents[14] have been reported. For the single crystal case, SCLC[5,6], double injection,[7] ionic and electronic carriers in different temperature ranges [8], and small polaron hopping[15] have been reported.

The above reports cover a variety of transport mechanisms for $BaTiO_3$ ceramic and single crystal, some of which apply to MLC capacitors. In addition, small polaron hopping reported for $LiNbO_3$[16] seems pertinent to the interpretation of our data.

The major types of current that we have seen are ohmic and SCLC. Ohmic current is proportional to voltage and can exist both for electronic (electrons and/or holes) and ionic carriers. The current-voltage relation is

$$I = q A n \mu V/L \qquad (1)$$

where q = electronic charge

A = area

n = carrier concentration

μ = drift mobility

If the electron density that results from injection from the cathode exceeds that native to the ceramic bulk, SCLC results. This current has a super-linear dependence ($I \alpha V^n$, $n > 1$), most typically varying as V^2. The current-voltage relation for planar electrodes and a shallow trap is[17]

$$I = \frac{9}{8} A \theta \varepsilon \mu V^2 / L^3 \tag{2}$$

where ε = permittivity

L = layer thickness

$$\theta = \text{trapping parameter} = \frac{N_c}{2N_t} e^{-\Delta E/kT} \tag{3}$$

N_c = conduction band density of states

N_t = shallow trap density

ΔE = trap energy, below conduction band edge

The injected charge for a metal on an n-type semiconductor consists of electrons. Even though the charge for SCLC originates from the electrodes, its transport depends totally on the ceramic bulk. Thus the ceramic bulk can be probed via SCLC.

Schottky, Poole-Frenkel, tunnelling and field emission currents depend exponentially on voltage. Even though MLC leakage currents have been attributed to Poole-Frenkel emission,[2] we have not detected currents with exponential voltage dependence, and these types are not discussed further.

We have also found a near $V^{3/2}$ voltage dependence, that is characteristic of new or weakly degraded devices. Precluding field dependent mobility, which is probably not a factor here, this behavior can be modelled on SCLC originating from point emitters. One possible current-voltage relation is[17,18]

$$I = \frac{2\pi\sqrt{2}}{3} \mu (\theta q \varepsilon n)^{1/2} V^{3/2} \tag{4}$$

where n is the native electron concentration and the other parameters were previously defined. The existence of such electrode emitters has been verified by cross sectional studies (discussed further in section 3.2).

2. LEAKAGE CURRENT MEASUREMENT

Most of these measurements were made on 1μF Z5U, and 10nF and 1μF X7R commercial capacitors. Some devices were obtained from vendors following accelerated lifetests (nominally at 125°C, twice rated voltage). We degraded additional capacitors of the same type under more accelerated conditions (typically at 180°C, at four or eight times rated voltage[4]).

2.1 Current-Voltage Behavior

Current-voltage measurements were made using a Hewlett-Pa d 6116A voltage supply and a Keithley 610B electrometer. Sample eratures were held to within about ±0.2°C, from room temperature to 200 .

Current decay is a problem for new devices at room temperature, and steady state leakage measurements across a wide voltage range are extremely difficult. An example of this is seen in Figure 1, where the current varies approximately inversely with the time. It is apparent that at least several hours would be required for the current to stabilize. This decay decreases substantially for new devices at elevated temperature; for this reason new devices were measured only in the 100-200°C temperature range.

An additional problem especially for Z5U devices, is the strong voltage dependence of dielectric constant near room temperature. Since space charge currents depend on dielectric constant, this voltage variation must be taken into account for I-V interpretation. This effect can also be largely precluded by performing the measurements at slightly elevated temperature. This is indicated in Figure 2, where C is plotted as a function of bias voltage at different temperatures for a 1μF Z5U device. It is seen that, even though the dielectric constant is quite

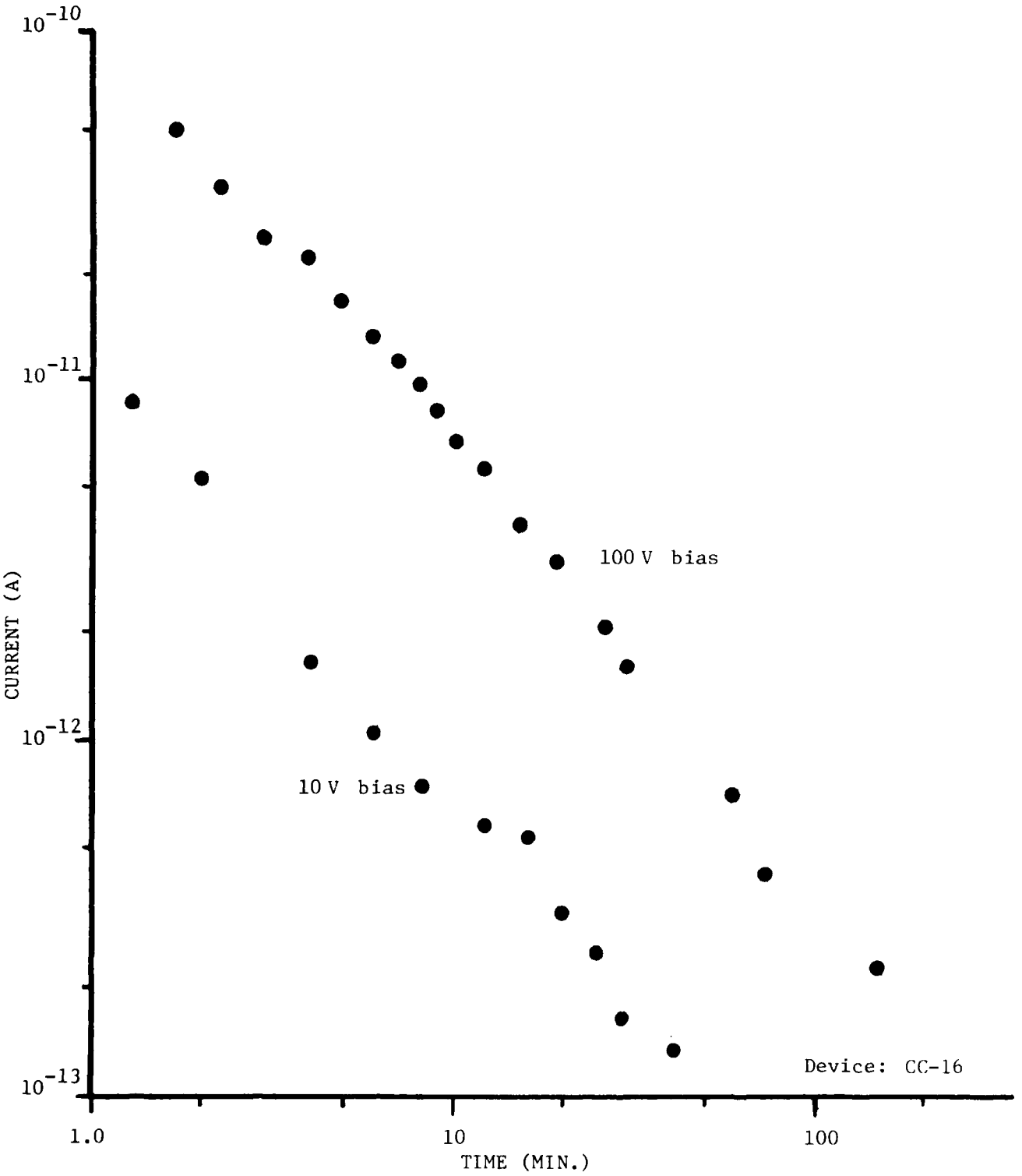

Figure 1. Current decay with time for new 10nF X7R capacitor, at 10 V and 100 V biases (room temperature).

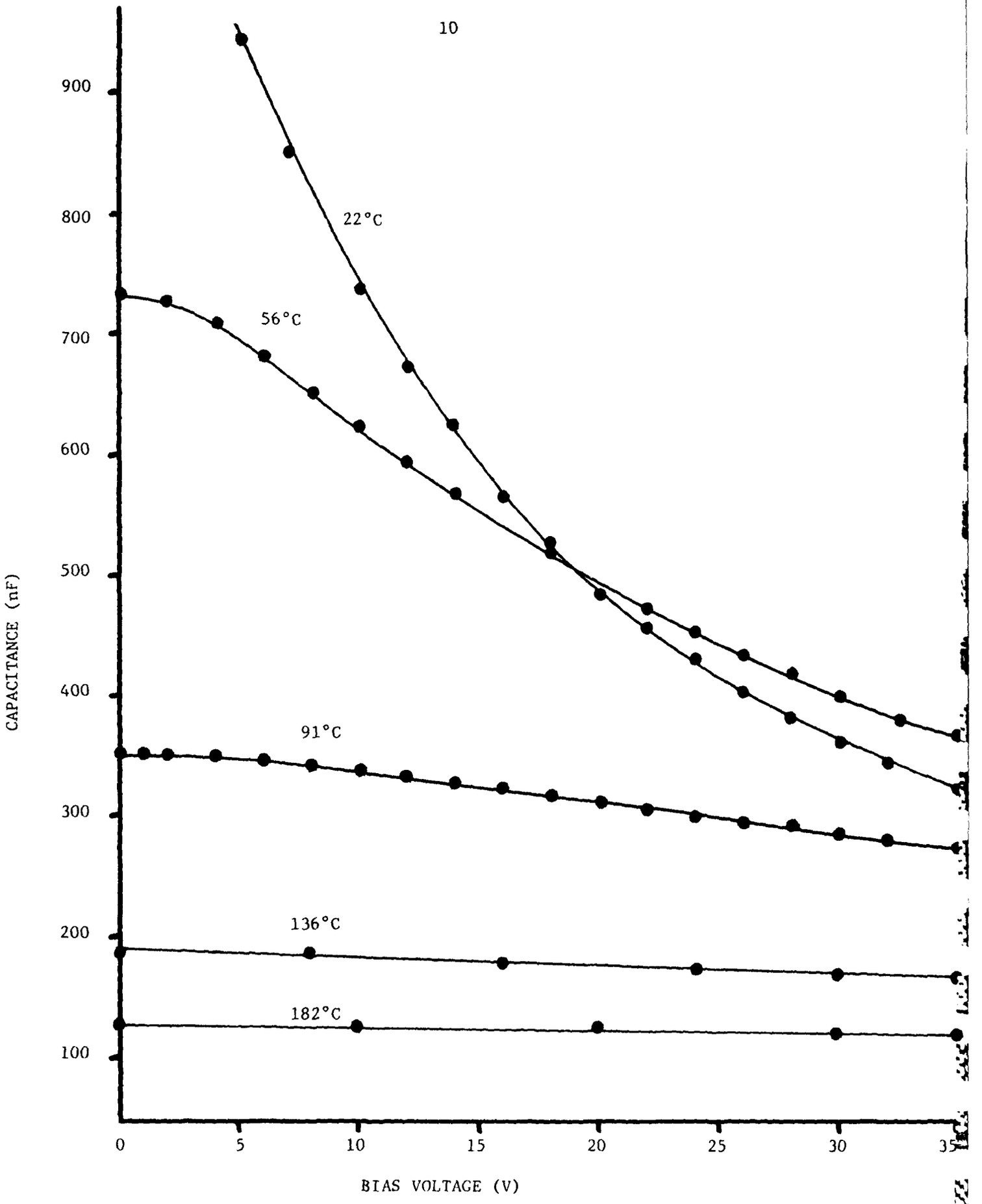

Figure 2. Capacitance (dielectric constant) versus bias voltage for a new 1μF Z5U device, at several temperatures. The dielectric constant becomes nearly independent of voltage above about 100°C.

substantially reduced, it becomes relatively voltage independent at temperatures above about 100°C. Therefore, most of the Z5U measurements were made at elevated temperatures for the above reasons. However, most of the results discussed below pertain to X7R capacitors, due mainly to their more extensive use in higher reliability applications.

A typical I-V curve for a new 1μF Z5U is shown in Figure 3. The near 3/2 power dependence of I on V, seen especially in the 50-100 V range, is common to all new Z5U and X7R devices measured. These measurements are very stable, drift free (at elevated temperature) and reproduceable. A possible model for the 3/2 power dependence is discussed below.

Aging a capacitor at elevated temperature and voltage increases its leakage current, and changes its I-V behavior. The latter shifts from a 3/2 or near -3/2 power behavior to ohmic (at low voltage) followed by quadratic SCLC behavior (at higher voltages.) Such a characteristic for a Z5U is seen in Figure 4. The upper part of this curve fits a V^2 behavior quite well, and is connected to the lower $V^{3/2}$ region by a sharply rising region indicative of trap filling. The hysteresis that is evident is also indicative that traps are full, and mobility increased, on the downward portion between about 5 and 1 volt. The sharper drop on the downward swing between 1 and 0.5 volts indicates that traps are being thermally emptied as the injected electron density decreases, with resultant decrease in mobility and hence current.

Activation energy analysis was not attempted for Z5Us, due to the strong temperature variation of dielectic constant, and the lesser importance of the Z5Us in our studies.

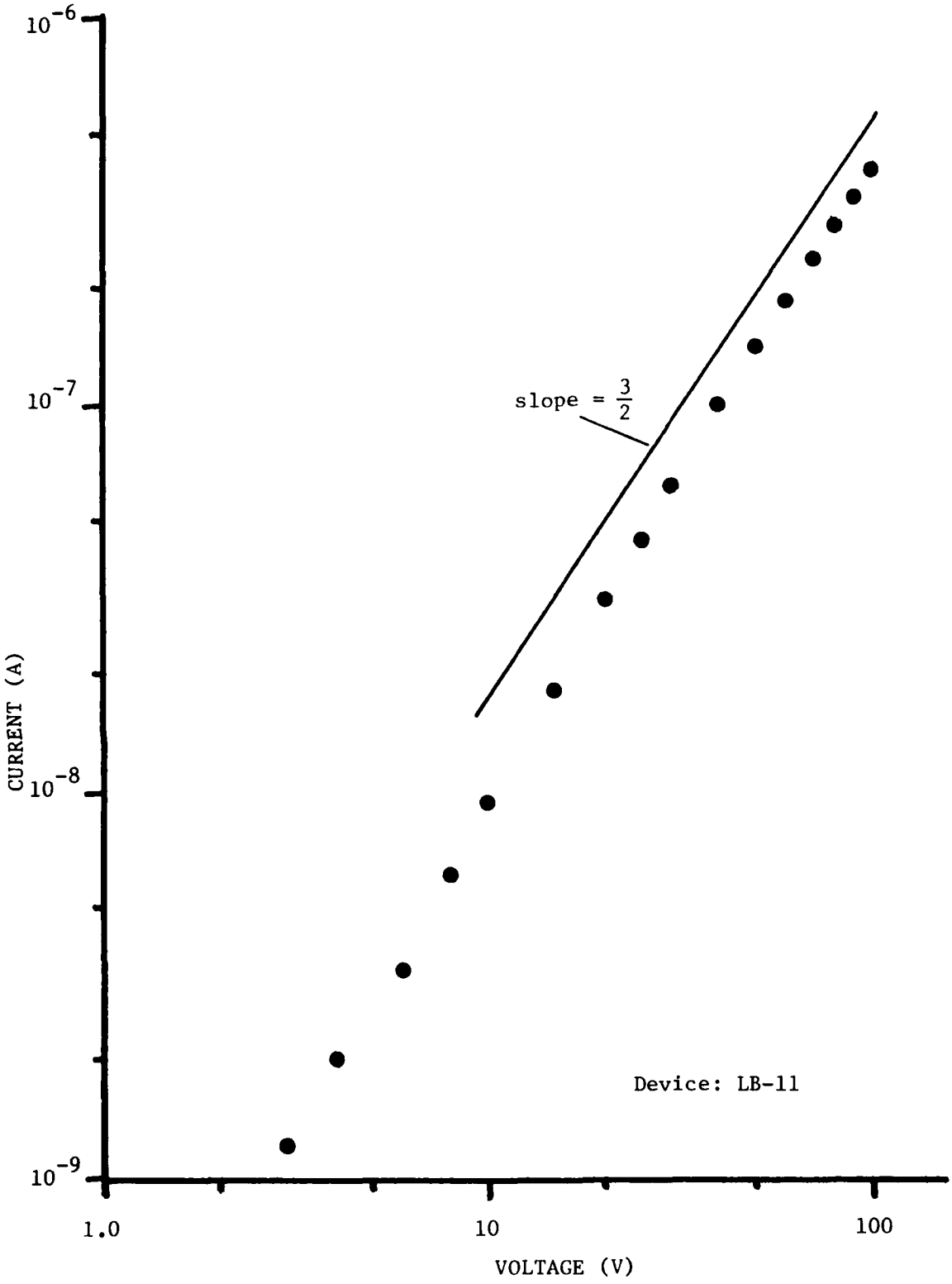

Figure 3. I-V curve for new 1μF Z5U, at T = 165°C.

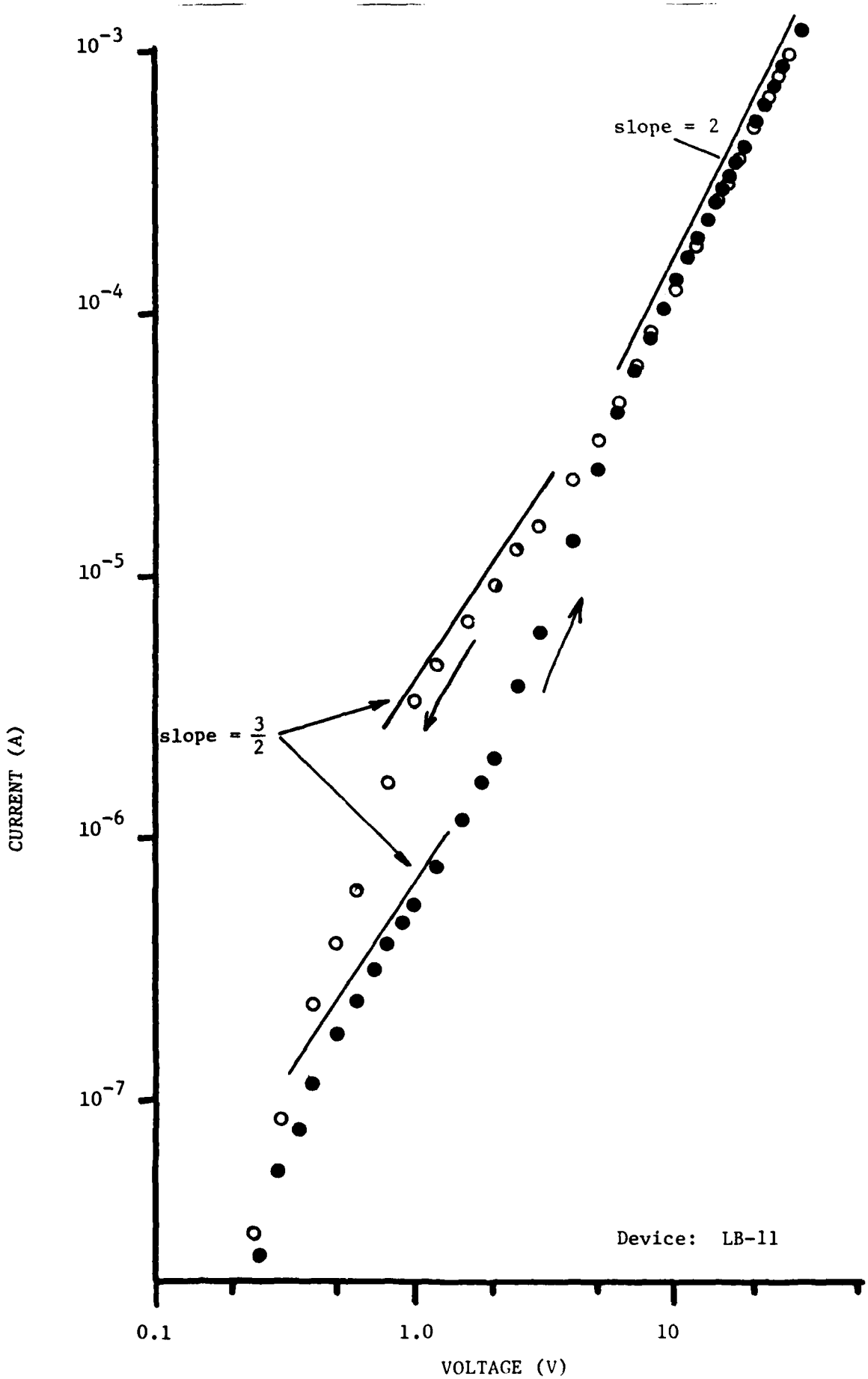

Figure 4. I-V characteristic for degraded 1μF Z5U, for voltage increasing (solid circles) and decreasing (open circles). T = 180°C.

All of the I-V results discussed from here on pertain to X7Rs. An I-V curve for a new 1μF X7R is shown in Figure 5. In this characteristic, $I \alpha V^{1.37}$. The I-V characteristic for this same device, after degradation (180°C, 400V) is shown in Figure 6. It consists of an ohmic region followed by a near 3/2 power region. Figure 5 represents a power law, which might be a form of space charge current described by emission from electrode protuberances, as described further below. An ohmic region was not apparent on any voltage range for a new device. The ohmic region developes during degradation (Figure 6) as the electron concentration in the ceramic increases. This raises the voltage where the transition from ohmic to space charge behavior occurs to a higher value. On a new device, because the electron concentration intrinsic to the ceramic is so low, the leakage current is controlled by electrode injection (i.e. is SCLC) over our entire voltage range (above 10mV). As the device degrades, an ohmic region becomes visible and in the limiting case, for very badly degraded devices, the entire I-V curve is ohmic (see Figure 14 below).

I-V curves for another new 1μF X7R are shown in Figure 7. These are all fairly close to a 3/2 power dependence. I-V characteristics of this same device, after degradation, are shown in Figure 8, where all 3 voltage dependences are clearly seen: ohmic (0.01-0.2V), 3/2 power (0.2-.8V) and square law (.8-10V). (Currents were not taken above about 10^{-4}A due to joule heating). The sharp increase in I at about 2-3 volts is attributed to trap filling. The square law behavior seen on either side of the trap filling increase is indicative of a shallow trap.

An I-V characteristic for a new 10nF X7R is seen in Figure 9. This characteristic is linear, with a $V^{1.44}$ dependence.

Activation energies for new and degraded X7R devices were determined by measuring I vs T at fixed voltage. An example for a new 10nF X7R is

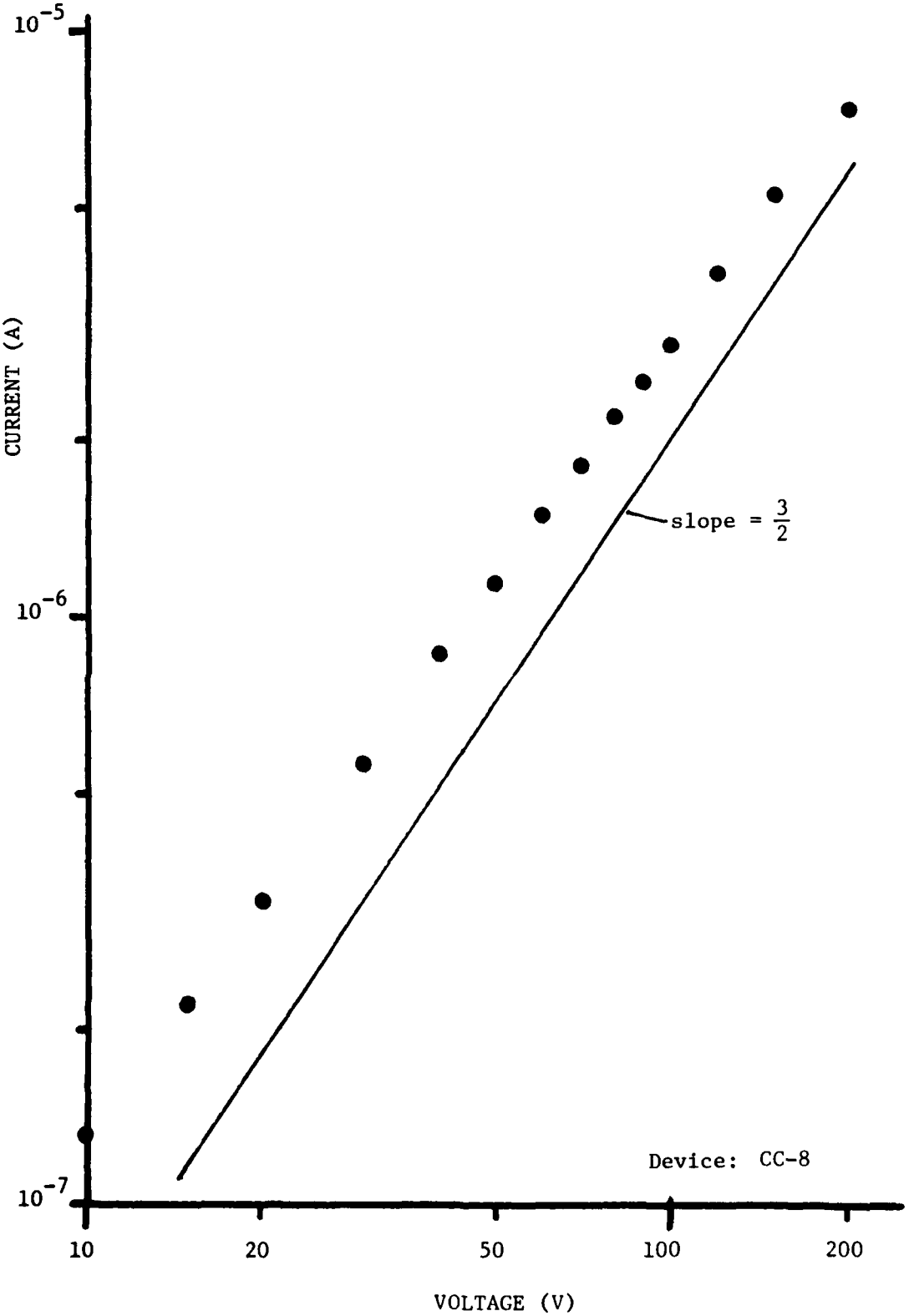

Figure 5. I-V characteristic for new 1μF X7R at T = 181°C.

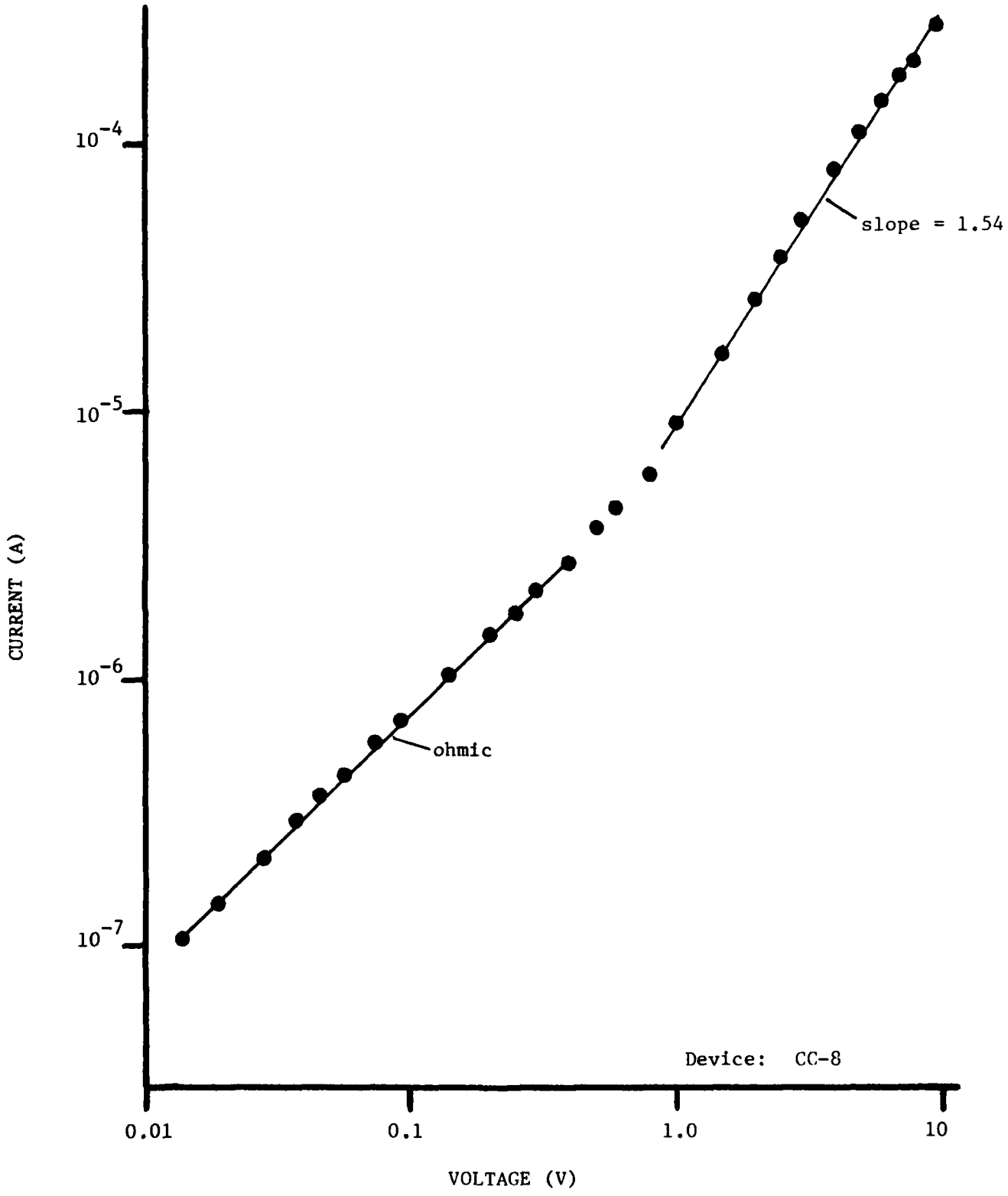

Figure 6. I-V characteristic for degraded 1μF X7R, at T = 23°C. (same device as Fig. 5)

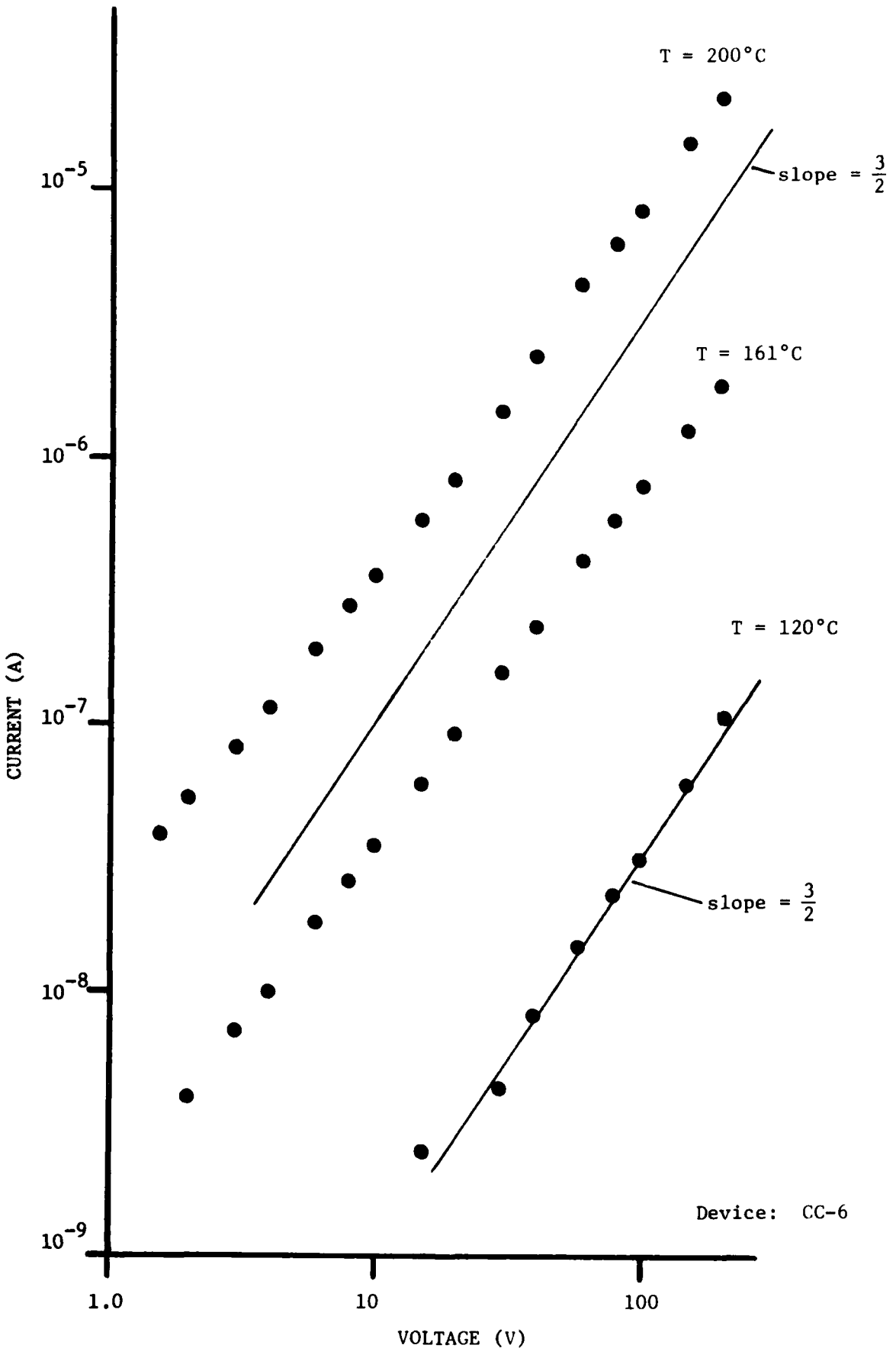

Figure 7. I-V curves for new 1μF X7R at several temperatures.

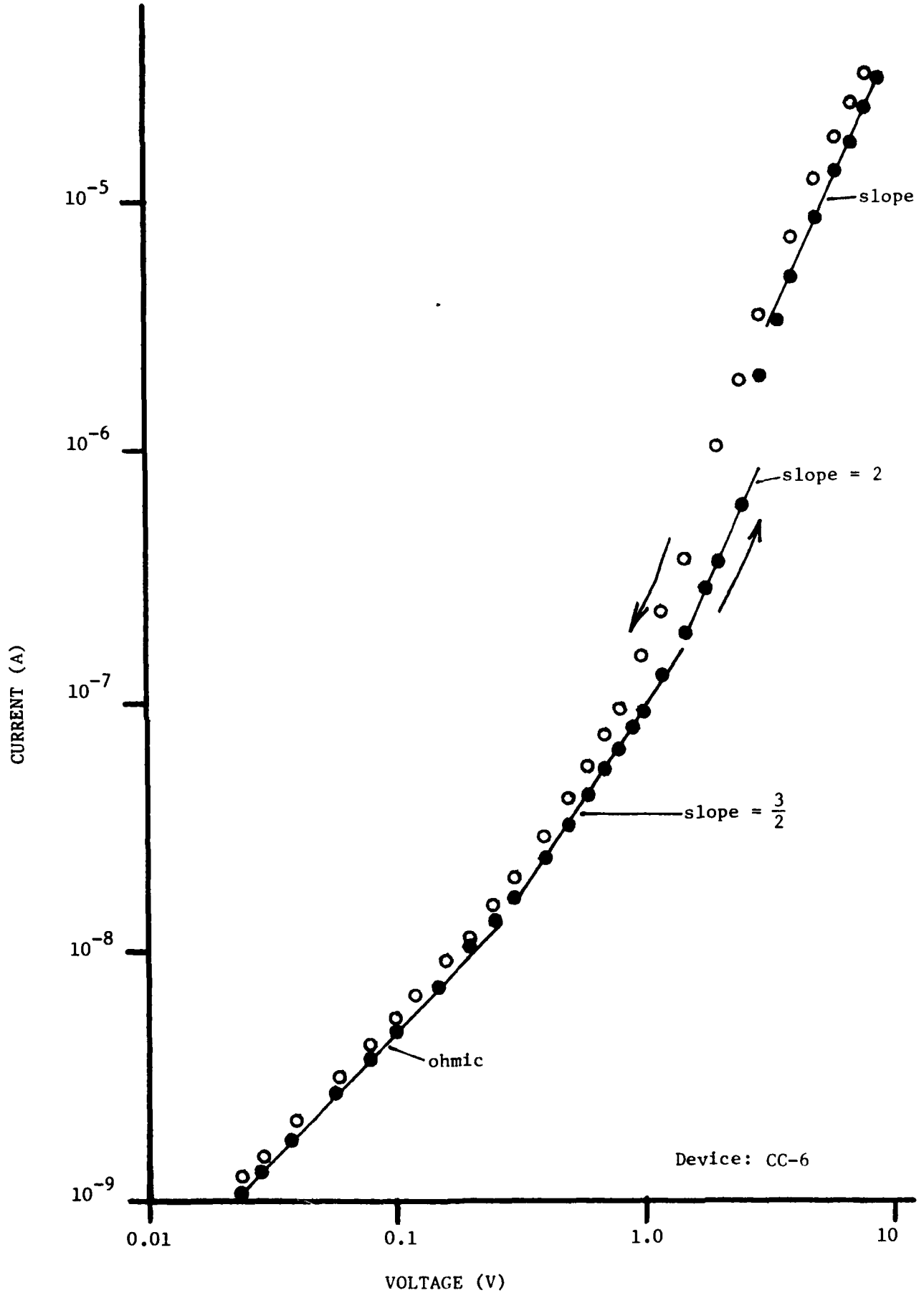

Figure 8. I-V characteristic for degraded 1μF X7R, at T = 23°C. (same device as Fig. 7)

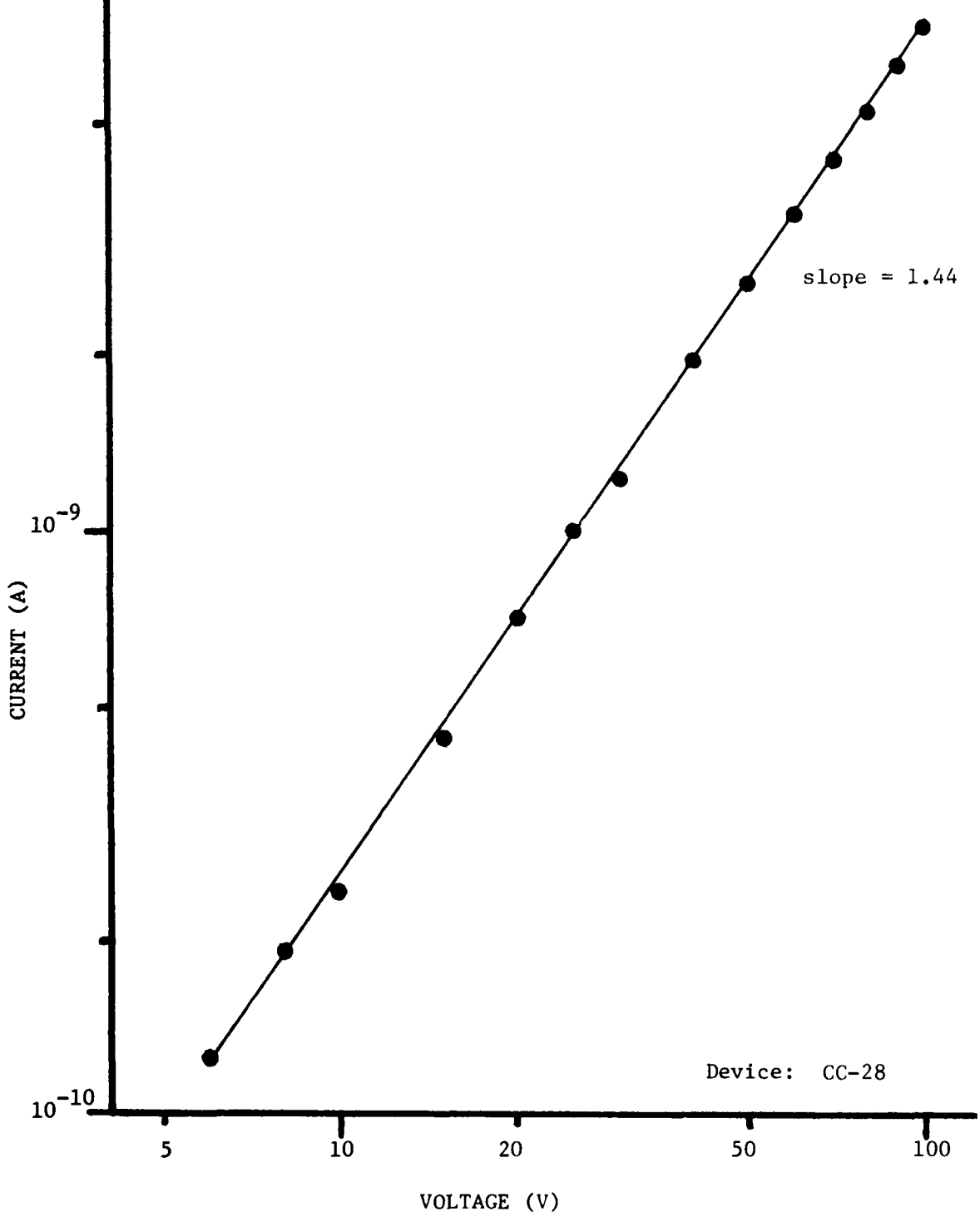

Figure 9. I-V characteristic for new 10nF X7R, with $V^{1.44}$ dependence. T = 162°C.

shown in Figure 10. Activation energies for new X7Rs are in the 1.2 - 1.3eV range. An I-V characteristic for this same device after degradation is shown in Figure 11.

The sharp increase at ~10-30 volts is attributed to trap filling. The square law behavior on either side of this trap filling increase indicates a shallow trap. The hysteresis indicates that the traps stay full on the downward cycle (note the similarity to the hysteresis seen in Figure 4 for a Z5U).

Even though obvious ohmic and space charge behavior were observed on many devices, anomalous voltage and time dependent behavior was also often seen. An example is shown in Figures 12 and 13. The initial runs on a degraded 10nF X7R are seen in Figure 12. An ohmic region followed by what appears to be trap filling and SCLC are evident on the lower curve. But the entire upper curve, as voltage decreases, is near ohmic. This should not be attributable to trap filling, since that should only effect the segment of the upper curve at voltages less than ~ 1 volt. However, the upper curve reverts back to the lower one after brief heating to ~ 100°C, indicating trap emptying.

After this device was heated to ~ 170°C during an activation energy run, it "healed" to the I-V characteristic seen in Figure 13. The leakage current decreased by some three orders of magnitude. This effect may be due to oxidation resulting from heating in air, or to other mechanisms, and may be a very localized effect. From studies of polished cross sections (discussed below) it is seen that there may be local inhomogeneities in the dielectric that could lead to localized leakage current. Since these regions can be quite small, they may be easily "healed" by local oxygen diffusion or by a joule heating fuse effect, which destroys the shunt.

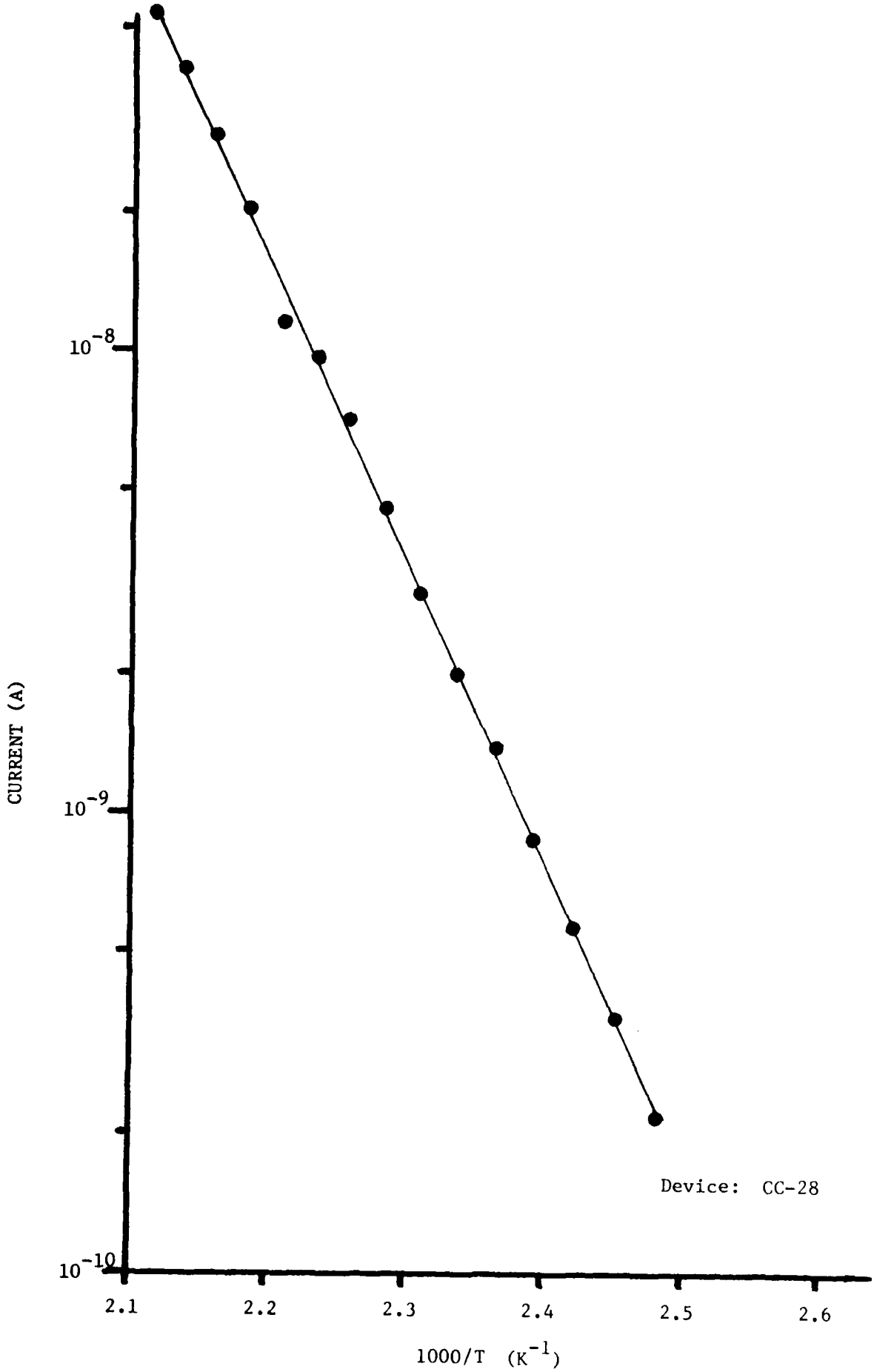

Figure 10. Arrhenius plot for new 10nF X7R. Activation energy is 1.26eV.

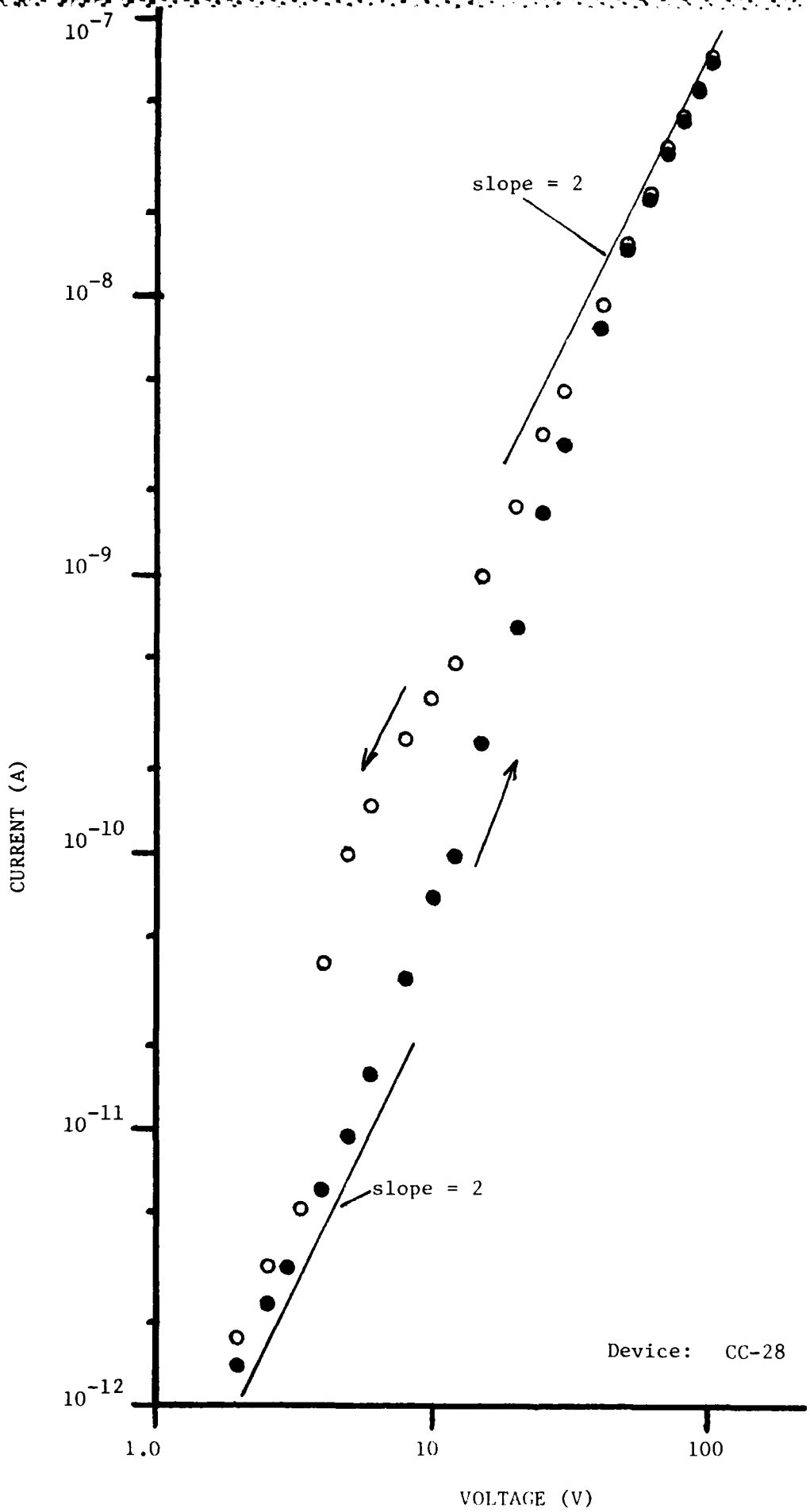

Figure 11. I-V curves for degraded 10nF X7R, at T = 22°C. (same device as in Figs. 9 and 10)

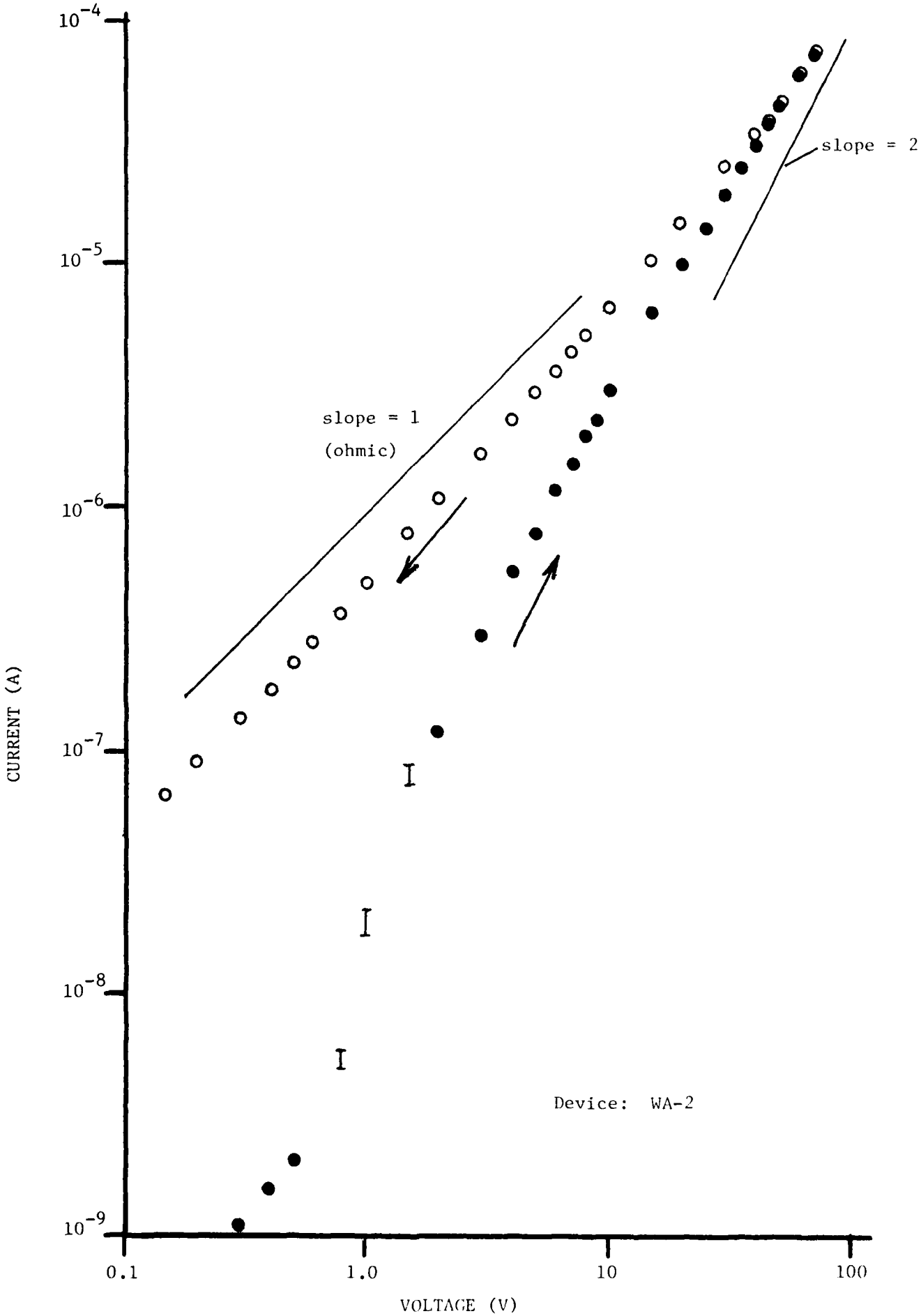

Figure 12. I-V curves for degraded 10nF X7R, at T = 22°C.

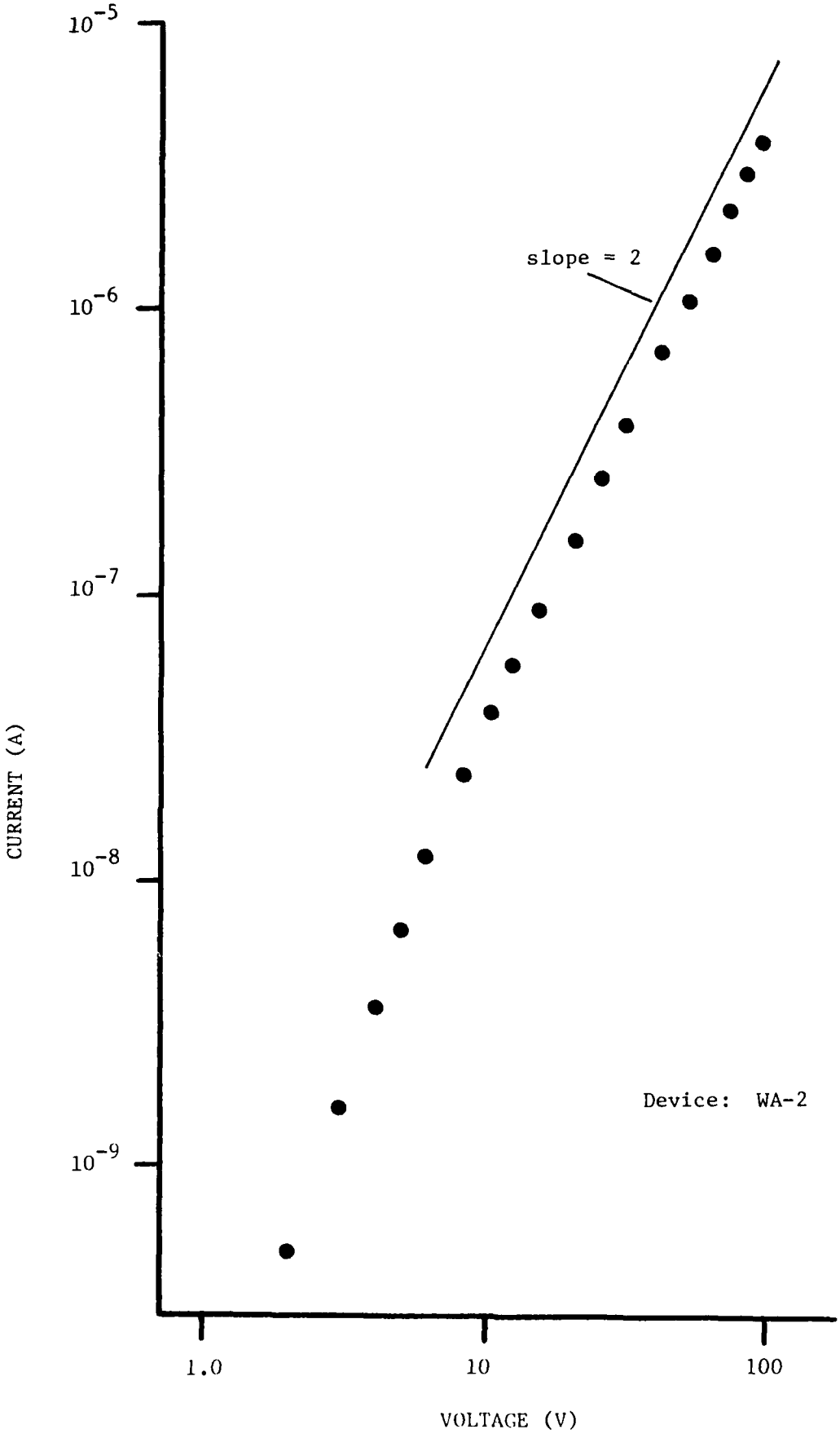

Figure 13. I-V curve for device of Fig. 12, after 170°C heating.

Severely degraded devices become ohmic over the entire voltage range. This is because localized shunts and/or native electron concentration become dominant over SCLC. If the native electron concentration becomes large enough, (due to $O^{=}$ diffusion for example) it exceeds the injected electron density for all voltages, and the latter is thus not seen. Examples are shown in Figures 14 and 15 for 10nF and 17pF X7Rs respectively.

Ohmic followed by space charge current was also seen for other size degraded X7R capacitors. This type of behavior is seen in Figures 16 and 17 for 144pF and 16pF devices respectively. For the 144pF device (Fig. 16), thermal activation energies were measured in the ohmic (at 0.1V) and SCLC (at 2V) regions. The activation energies were 0.162eV and 0.107eV. The lower activation energy in the SCLC region is consistent with the fact that this current is proportional to mobility, whereas the ohmic current is proportional to mobility and native carrier concentration. This indicates that the mobility activation energy (for the 144pF device) is 0.107eV and the native carrier concentration activation energy is 0.162 - 0.107 = 0.055eV.

Thermal activation energies (ϕ) were always less for degraded devices. This decrease in ϕ is shown in Figure 18, where ϕ is plotted versus resistivity (at 125°C, for X7R devices). Degraded devices with activation energies near zero have resistivities of about $10^5 \Omega$ cm. or less, and are ohmic. For 10nF devices, with area to thickness ratio of about 60, this corresponds to a insulation resistance of roughly 2 KΩ or less.

A caveat should be mentioned concerning these "resistivity" values. They were computed by knowing current, voltage and device dimensions, in an ohmic region, if possible. However, there are two reasons why they are, at best, approximations.

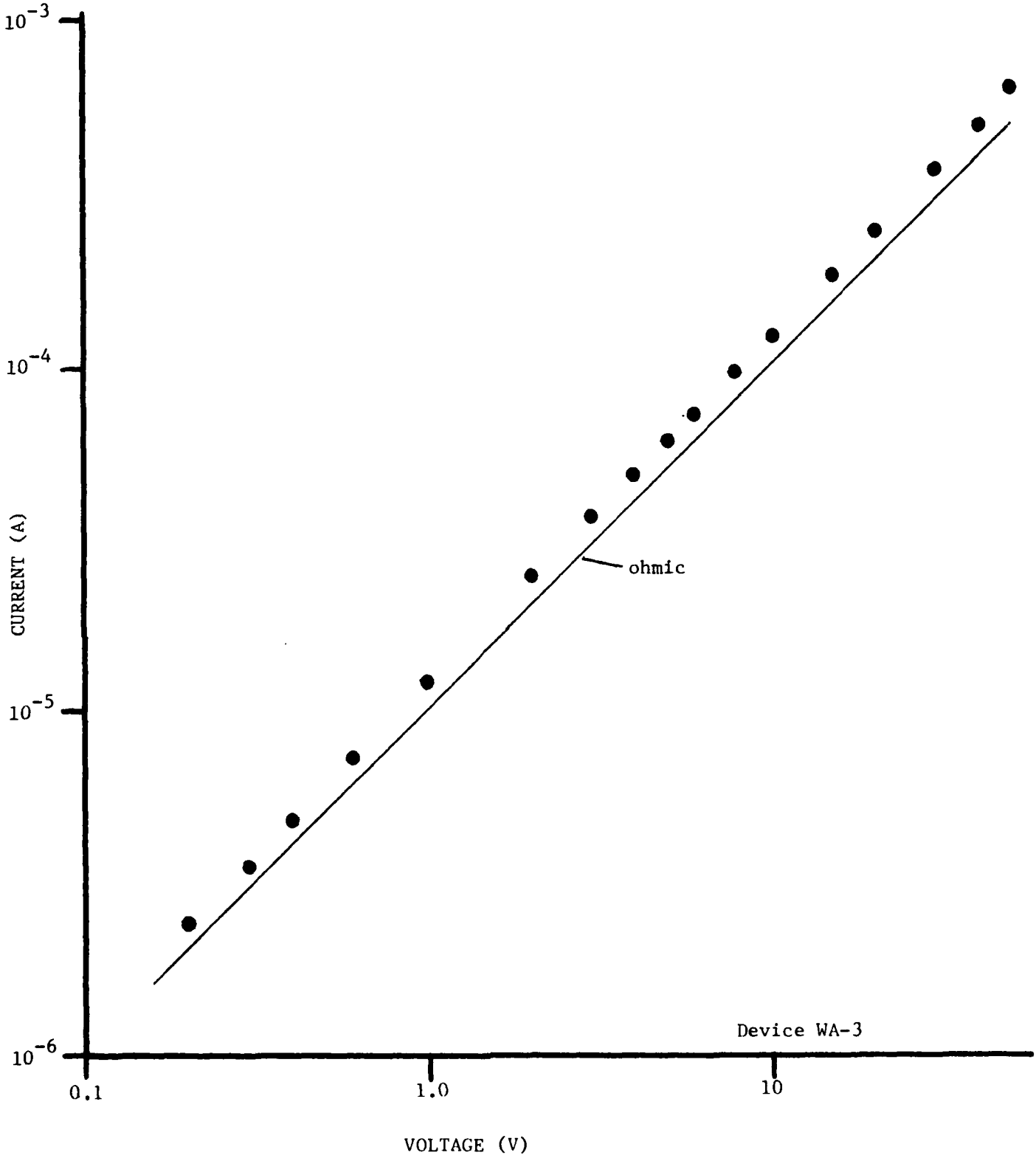

Figure 14. I-V curve for severely degraded 10nF X7R, indicating ohmic behavior (T = 22°C).

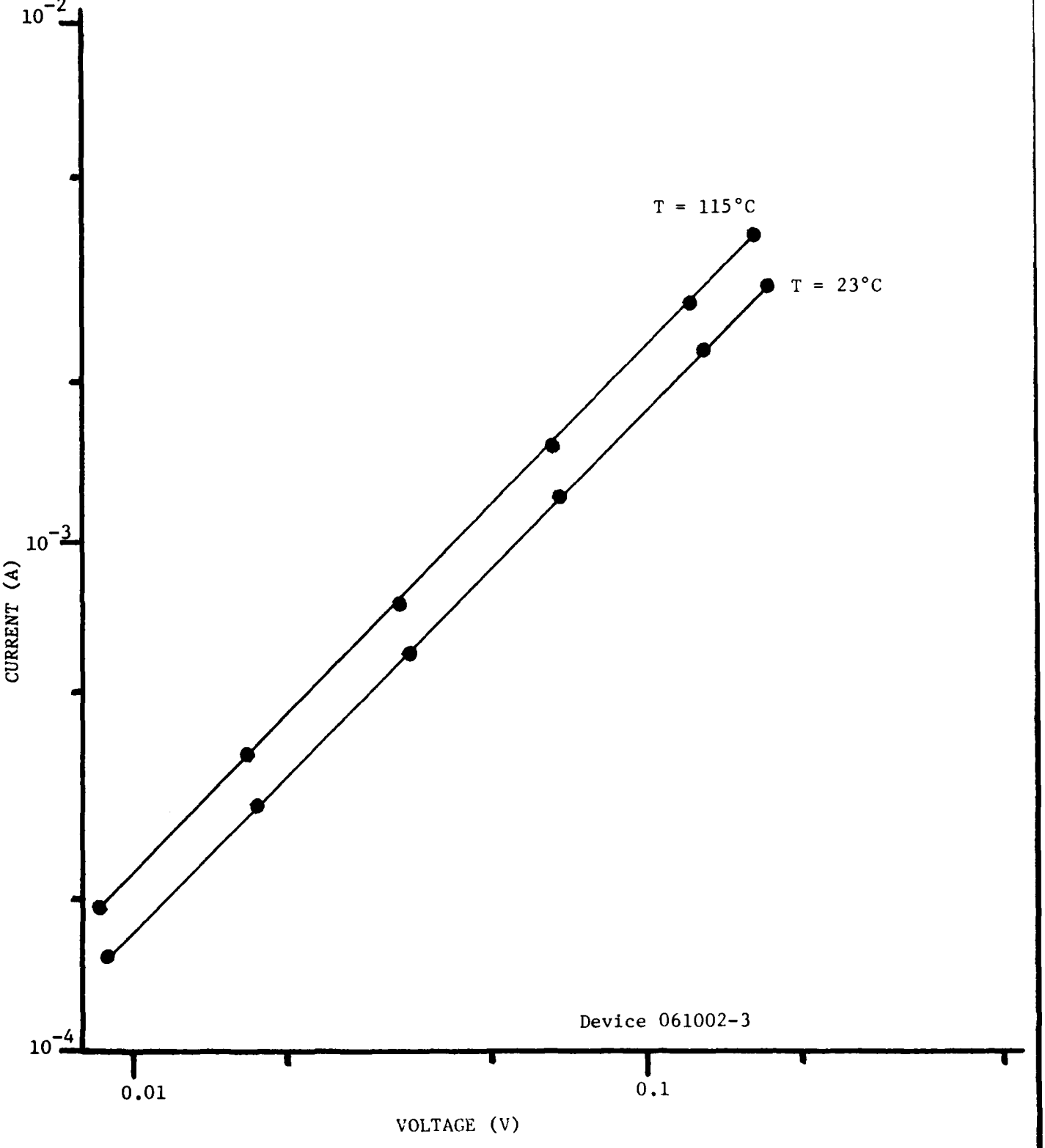

Figure 15. I-V curve for severely degraded 17pF X7R, at two temperatures.

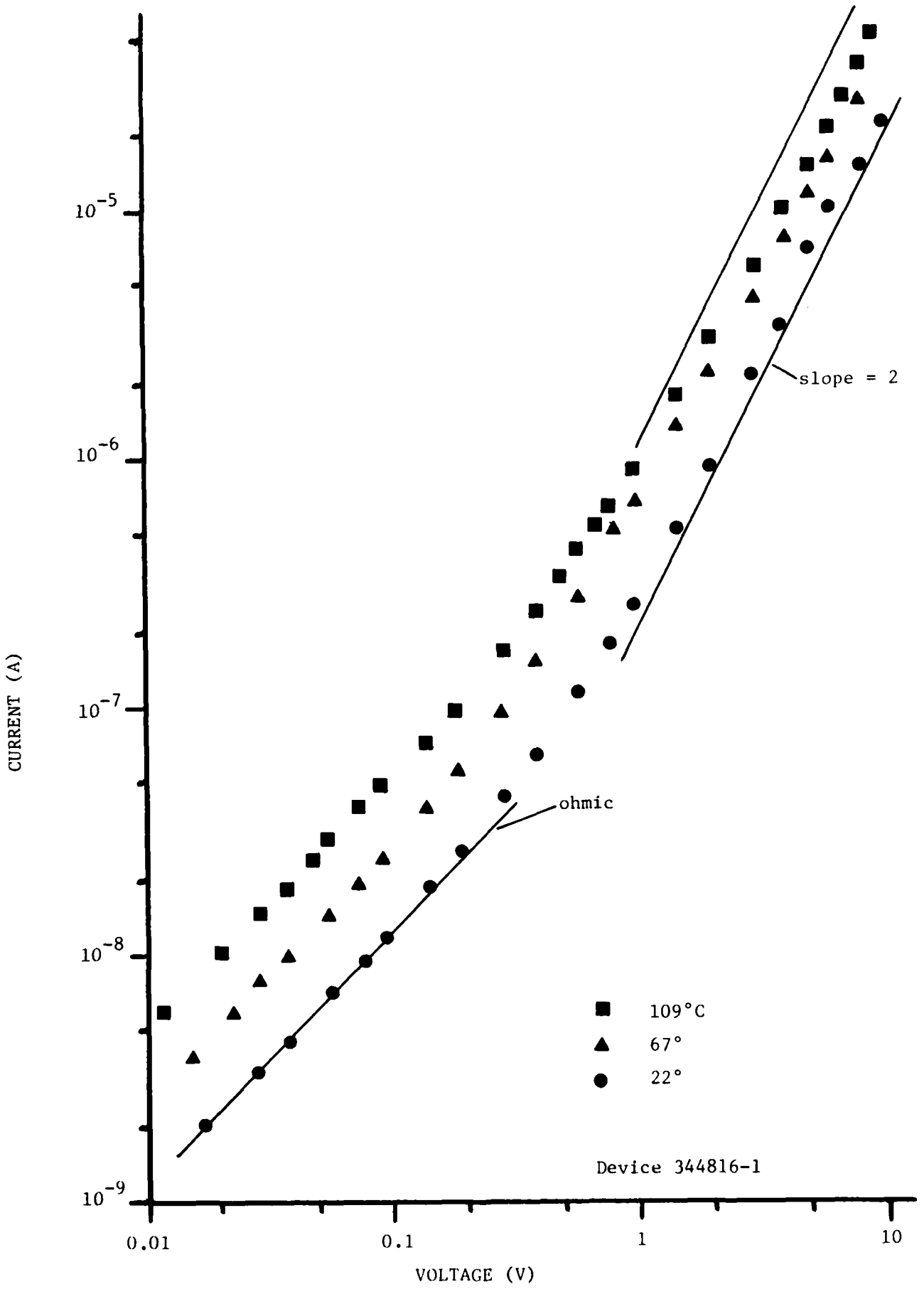

Figure 16. I-V characteristic for degraded 144pF X7R, at three temperatures.

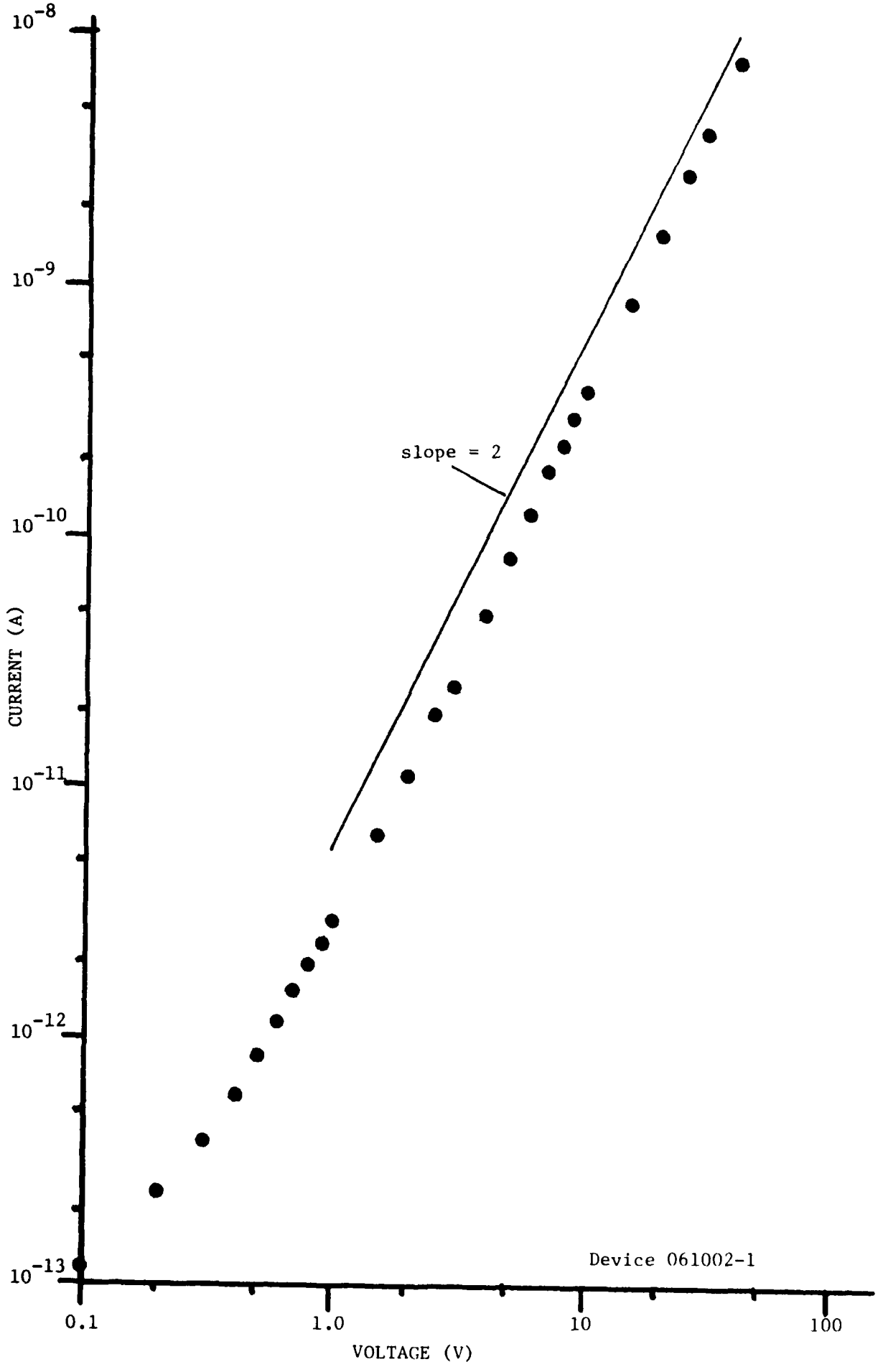

Figure 17. I-V curve for degraded 16pF X7R.

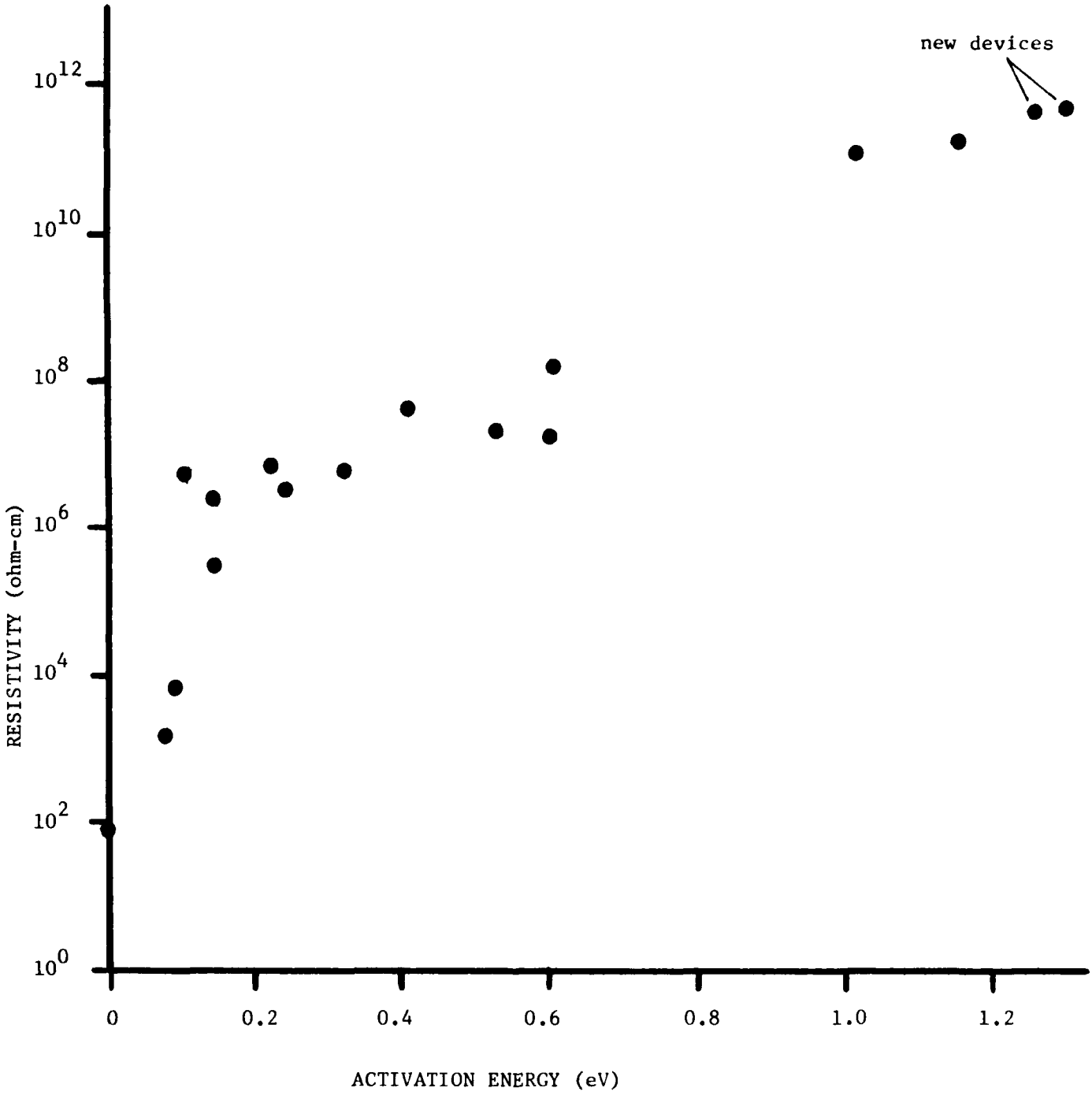

Figure 18. Resistivity versus thermal activation energy for X7R devices (Resistivity values at 125°C.)

i) In a new device, a truly ohmic region could not be distinguished, and the "resistivity" therefore (as defined by the relation $V/I = \delta \ell/A$, δ being the resistivity) is a function of voltage. Degraded devices do not have this problem, since an ohmic region can generally be found at lower voltages.

ii) As will be discussed in the next section, devices degraded under DC conditions most probably have a resistivity gradient across the dielectric.

The thermal activation energy ϕ shown in Figure 18 can be broken down into two parts, since conductivity can be expressed as

$$\sigma = q\, n\, \mu = \sigma_0\, e^{-\phi/kT} = q\, n_0\, \mu_0\, e^{-(\phi_n + \phi_\mu)/kT}$$

Thus $\phi = \phi_n + \phi_\mu$ represents the sum of activation energies for carrier concentration generation and drift mobility increase. We will discuss this in greater detail in section 4, where it will be shown that the decrease in resistivity for reduced X7R ceramic can be attributed to a mobility increase, accompanied by an electron concentration increase, with the temperature dependence residing almost entirely in the mobility.

2.2 Parameters Deduced from SCLC

What quantitative information about the dielectric can be obtained from a space charge current-voltage characteristic? Rough estimates for drift mobility, trap concentration and trap energy can be obtained as follows: Consider the generic SCLC characteristic shown in Figure 19, for the case of shallow traps.

Assuming that the steep characteristic is due to trap filling at voltage V_T, equation 2 can be solved for mobility:

$$\mu \approx \frac{IL^3}{A\theta\varepsilon V_T^2} \tag{5}$$

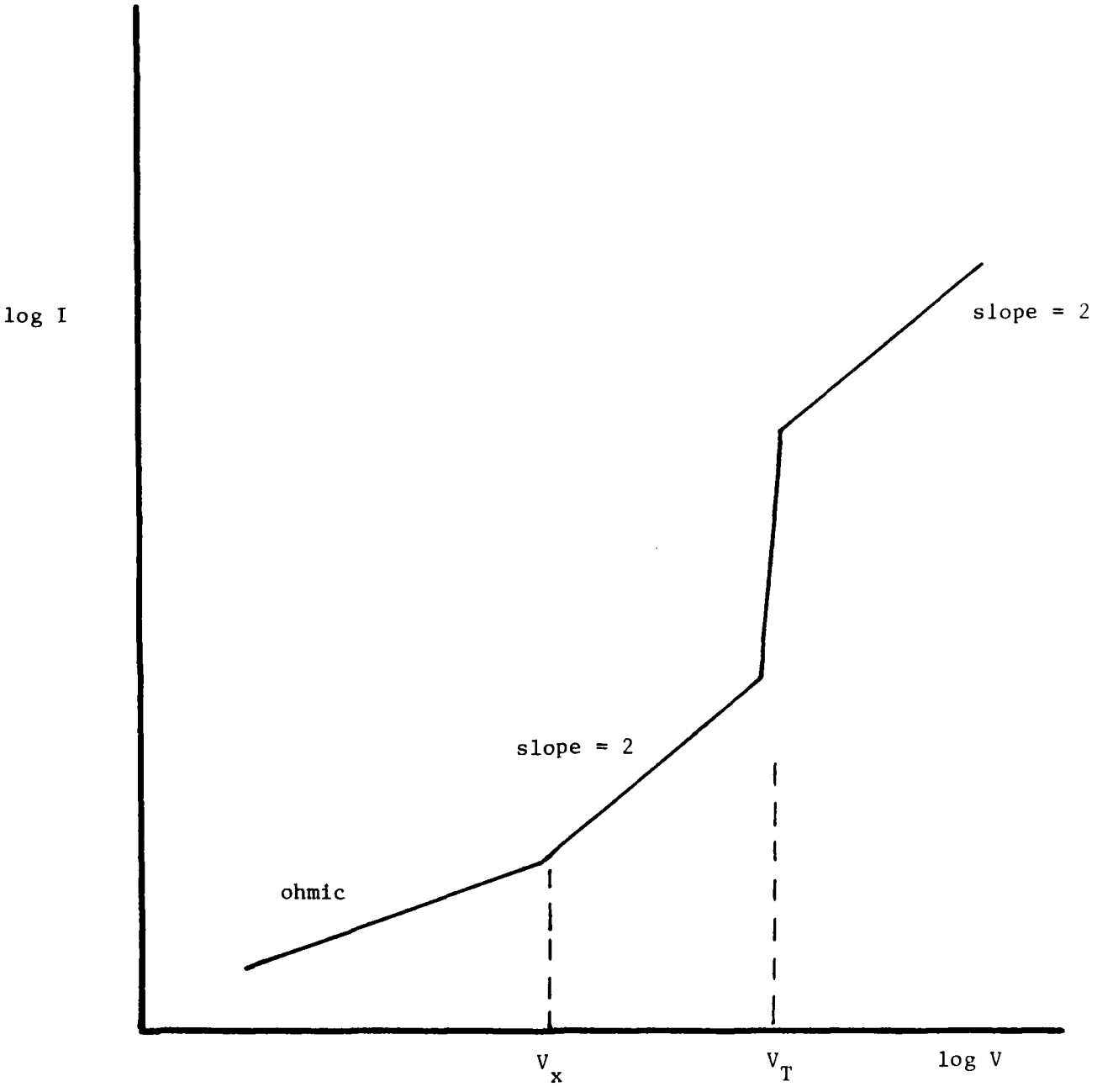

Figure 19. Generic current-voltage characteristic illustrating ohmic, square law and trap filling behavior.

The trap density can be estimated from the relation[17]

$$N_t \approx \frac{10^6 \, K \, V_T}{L^2} \tag{6}$$

where K is dielectric constant. The distance of the trap from the conduction band edge can be obtained from equation 3 as

$$\Delta E = kT \, \ell n \, \frac{N_c}{2\theta \, N_t} \tag{7}$$

For 10nF X7R devices that exhibit I-V characteristics similar to those of Figure 19, and using $A = 0.36\,cm^2$, $L = 0.006\,cm$, and $\varepsilon = 1.8 \times 10^{-10}$ F/cm, we have made the following estimates for μ, N_T and ΔE:

Mobility: $10^{-7} < \mu < 10^{-2}\,cm^2/Vsec$

Trap concentration: $10^{14} < N_T < 10^{15}\,cm^{-3}$

Trap location: $0.4 < \Delta E < 0.6eV$

The smaller mobility values correspond to less severely degraded devices. These low values, combined with the exponential dependence of μ on temperature, are characteristic of electron hopping.

The large mobility range given above results from equation (5), due to the large increase in I as devices degrade, with V_T usually remaining in the 1-10V range. This is consistant with the fact that the ohmic and SCLC regions both increase as a device degrades, each being proportional to mobility. If only the carrier concentration increased during degradation, (and if mobility remained constant), then only the ohmic part of the current would increase; V_x of Figure 19 would increase and the SCLC current (for $V > V_x$) would be unchanged. This is because the SCLC does not depend on the background carrier concentration in the ceramic, but on

electrode emission, and, for transport, drift mobility. This implies that a mobility increase is just as significant as a carrier concentration increase as a device degrades. Evidence to support this, from thermoelectric measurements, will be discussed in section 4.

Some comments should be made about the validity of the above estimates in light of the probable non-uniformity in dielectric properties (see Figure 20).

i) The color gradient seen across the dielectric indicates a resistivity gradient. This would tend to broaden the transition from ohmic to space charge behavior, since space charge currents will dominate only when the injected electron concentration exceeds that everywhere in the ceramic. This might account for the somewhat rounded value of V_x often seen.

ii) The mobility is almost certainly a function of position between the electrodes. Since the regions of varying mobility are in series, the smaller values will dominate the current, and will tend to make the deduced mobility appear to be less than the average value.

The above parameters, arrived at from space charge characteristics, are therefore <u>at best</u>, only estimates, that should be complemented by additional independent measurements. However, their orders of magnitude are similar to those reported for $BaTiO_3$ single crystal[5,6]. The similarity of results for $BaTiO_3$ single crystal and X7R ceramic seems to indicate that grain boundaries do not play a dominant role in charge transport in these devices. This is also indicated by our thermoelectric results, which are similar to those reported for single crystal[15], and by the fact that the frequency dependence of the dielectric constant and loss do not change significantly for even quite

severely degraded devices. Since mobility appears to increase quite drastically with degradation, this increase is apparently not caused by reduced grain boundary potential, but by reduced hopping potential in the bulk of the grain. Hence the similarity between these results and those reported for single crystals.

2.3 3/2 Power Model

We would now like to discuss one possible model for the 3/2 or near -3/2 power dependence of leakage current on voltage for new or mildly degraded devices, both Z5U and X7R.

It is known that electron emission into a solid from a hemispherical electrode can be described by a 3/2 power law[17,18], as indicated in equation 4. (The 3/2 power dependence on voltage for emission from a planar cathode into a vacuum does not apply here.) Emission similar to that described by equation 4 could conceivably occur from electrode non-uniformities, bumps, points and protuberances. (Examples are shown in the next section.) There are potentially a large number of these emitters in a given MLC device, since we have found several as a result of only a very limited amount of cross sectioning. The enhanced field that will exist at the tip of such an emitter must be viewed as a possible major source of device degradation, since both local joule heating (due to increased current density near the tip) and oxygen ion diffusion (due to the larger field and the heating) will be enhanced.

Such a model should also address the question as to why the 3/2 power dependence transforms into a higher power (commonly quadratic) as the device degrades. Consider an electrode where protuberances originate due to the existence of ceramic pores, grain boundaries, etc., adjacent to the electrode. (See Figure 32). The field at the protuberance

tip will be much larger that at the more planar cathode region. Oxygen ions will diffuse away from the tip preferentially, and a lower resistivity region will thus spread outward from the tip (the type of color gradient seen in Figure 20 will be accentuated). The electric field in this reduced region will be decreased, because current density continuity requires that

$$J = \sigma_1 E_1 = \sigma_2 E_2, \text{ where } E = \text{electric field;}$$

i.e. $E_2/E_1 = \sigma_1/\sigma_2$, and the higher conductivity region will have the lower field. Thus, the effective tip radius will increase, the field will decrease and the 3/2 power emission becomes less predominant. For small protuberances (such as seen in Figure 32) this effect would tend to eventually nullify the enhanced emission from the tip, and the electrode would appear nearly planar, with a quadratic type of voltage dependence taking over. Simultaneously, the overall resistivity of the ceramic layer has, on the average, decreased, and overall current increased. Thus, one might expect, if this model is correct, a transformation from near 3/2 power to square law voltage dependence, accompanied by increased leakage current. That this is what is observed in many cases does not confirm the model, since the model is certainly not unique. Other field dependent models are available [19-21], but seem even more speculative than this one.

3. CROSS-SECTIONED CAPACITORS

Scanning electron and optical microscope studies, and compositional measurements using EDAX, AES and electron beam microprobe were made on cross-sectioned X7R and Z5U devices.

3.1 Dielectric Defects

Optical microscopy revealed color differences between new and degraded devices. New capacitors have overall uniform color between electrodes. Figure 20 shows an obvious color gradient across the ceramic for a degraded Z5U device (seen here in black and white). This picture was made on a thin polished slice, using transmitted light. This effect can also be seen using reflected light, but is not as dramatic as for transmitted light.

The use of polarized reflected light also indicates a color difference for material between the electrodes and external to the electrodes (Figure 21). This effect is seen for both new and degraded capacitors and is apparently an optical shading effect. The fact that it does not appear in the ceramic external to the electrodes, even adjacent to an end electrode, indicates that it is probably not a result of diffusion of electrode ink components. Compositional differences between these regions are not distinguishable using the above spectroscopies.

Light colored regions were also visible under polarized light (Figure 22). When this surface was preferentially etched (using 5% HCl + 0.05% HF) to bring out the grain structure, the light colored area is seen to represent a region of small grains surrounded by second phase material (Figure 23). This small grained region is seen more distinctly in the SEM shown in Figure 24. Such areas of small grains appear to be

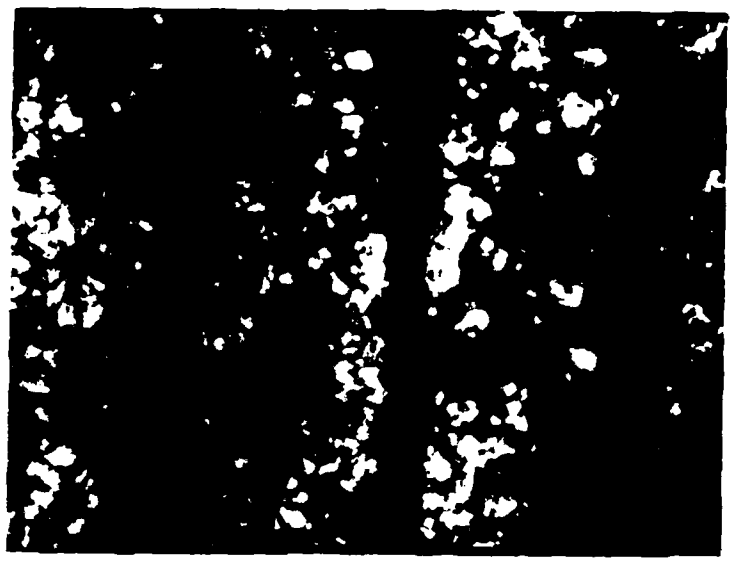

Figure 20. Color gradient (here in black and white) between electrodes of degraded Z5U; transmitted polarized light at 500X.

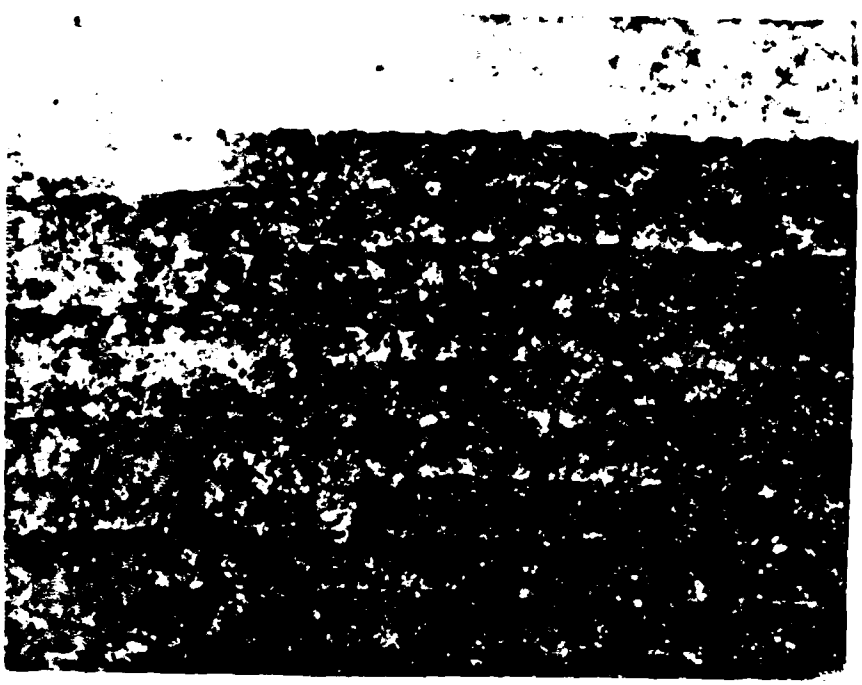

Figure 21. Degraded Z5U; reflected light at 260X.

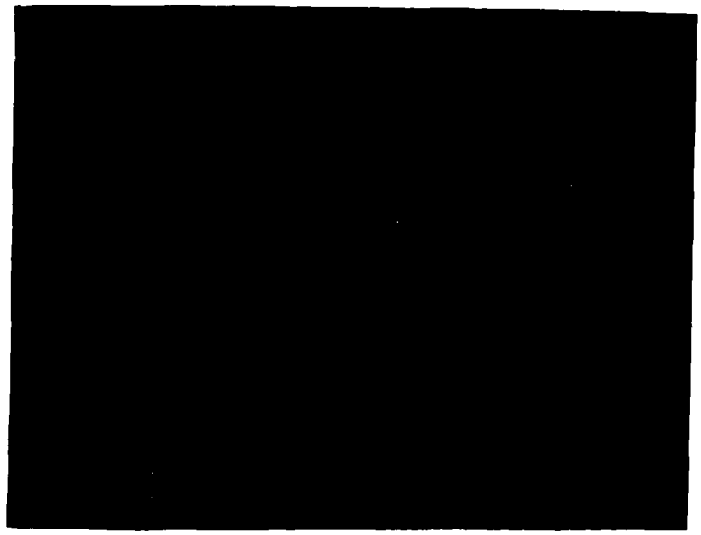

Figure 22. Light region on new Z5U (original in color); reflected polarized light at 400X.

Figure 23. Same region as in Figure 22 after decorative etch; unpolarized light at 400X.

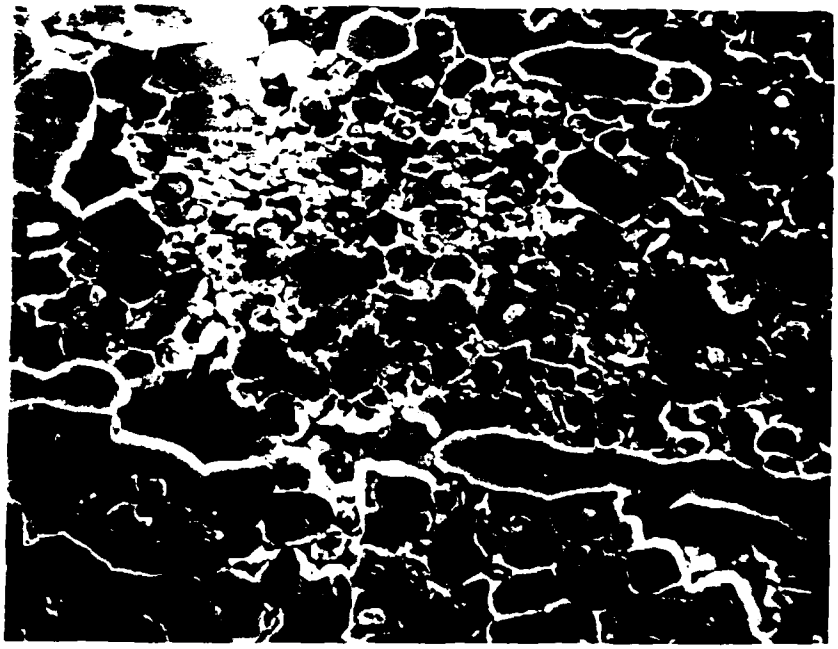

Figure 24. SEM picture of region shown in Figures 22 and 23; magnification = 2000.

randomly distributed in the dielectric. The SEM also indicates what is apparently a second phase region. EDAX done on several specimens reveals the grains to be primarily barium titanate, with zirconium and calcium. EDAX on the second phase material shows it to have higher levels of Zr and Ca, with Zn also present. Figure 25 shows a second phase region (upper part of picture) and Figure 26 shows an EDAX spectrum, and the presence of Zn in the second phase. The presence of Zn in the second phase was confirmed by microprobe analysis. Microprobe zinc maps for new and degraded Z5U devices are shown in Figure 27. Localized concentrations of Zn are evident in both cases.

Auger, EDAX and microprobe analyses were used to try to discern compositional gradients between electrodes caused by ionic migration, and to compare new and degraded devices. Typical AES spectra can be compared in Figures 28A and 28b. A large number of such spectra were taken, some accompanied by ion-milling to remove surface damage. However, no conclusive compositional differences or gradients caused by accelerated lifetests on devices of the same type could be identified.

Areas of second phase material were also found on cross sectioned Z5U devices from a second vendor. An example is seen in Figure 29. SEM reveals the second phase more clearly (Figure 30a) EDAX spectra for the mid-grain and second phase locations indicate that the second phase is rich in Cd. These spectra are shown in Figure 30b and 30c.

The resistivities and dielectric constants of these Zn and Cd rich regions are not known. If these parameters vary, the electric field distribution would also vary, somewhat, but not as extensively as in a pore. This could have an adverse effect on the lifetime of the device. The origins of these inhomogeneities are not known.

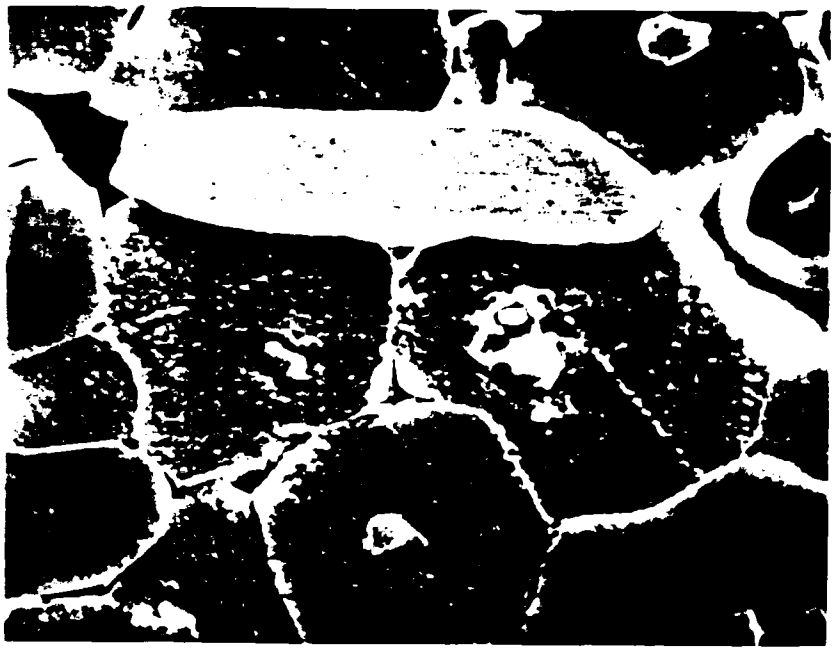

Figure 25. SEM (5000X) on new Z5U indicating second phase region in upper part of picture.

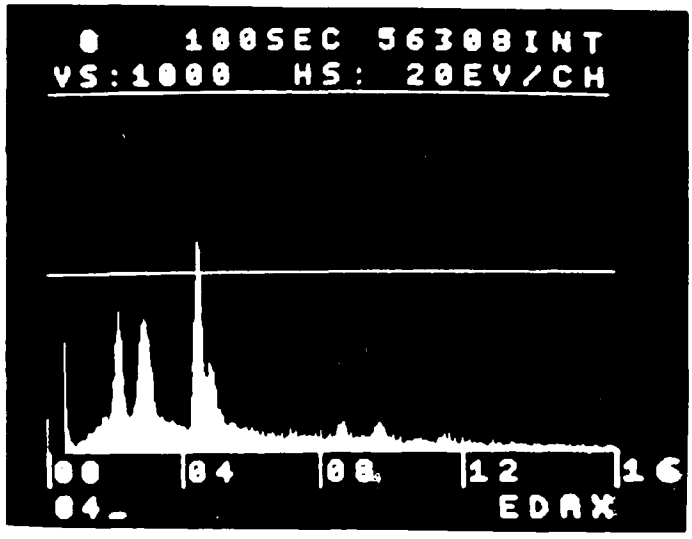

Figure 26. EDAX spectrum indicating Zn in the second phase region. (Mid grain spectrum had no Zn peak.)

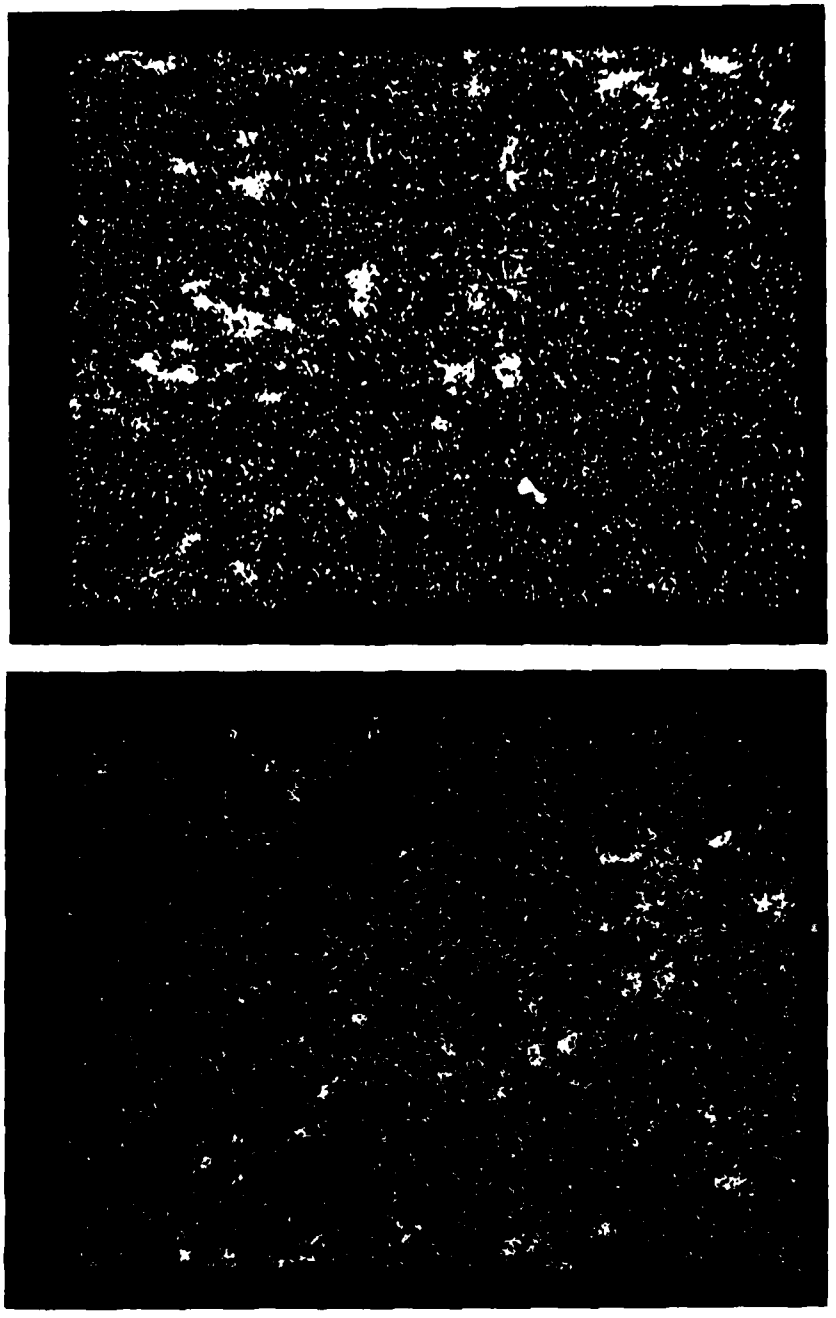

Figure 27. Microprobe Zn maps for new (upper) and aged (lower) Z5U capacitors. Magnification = 1000.

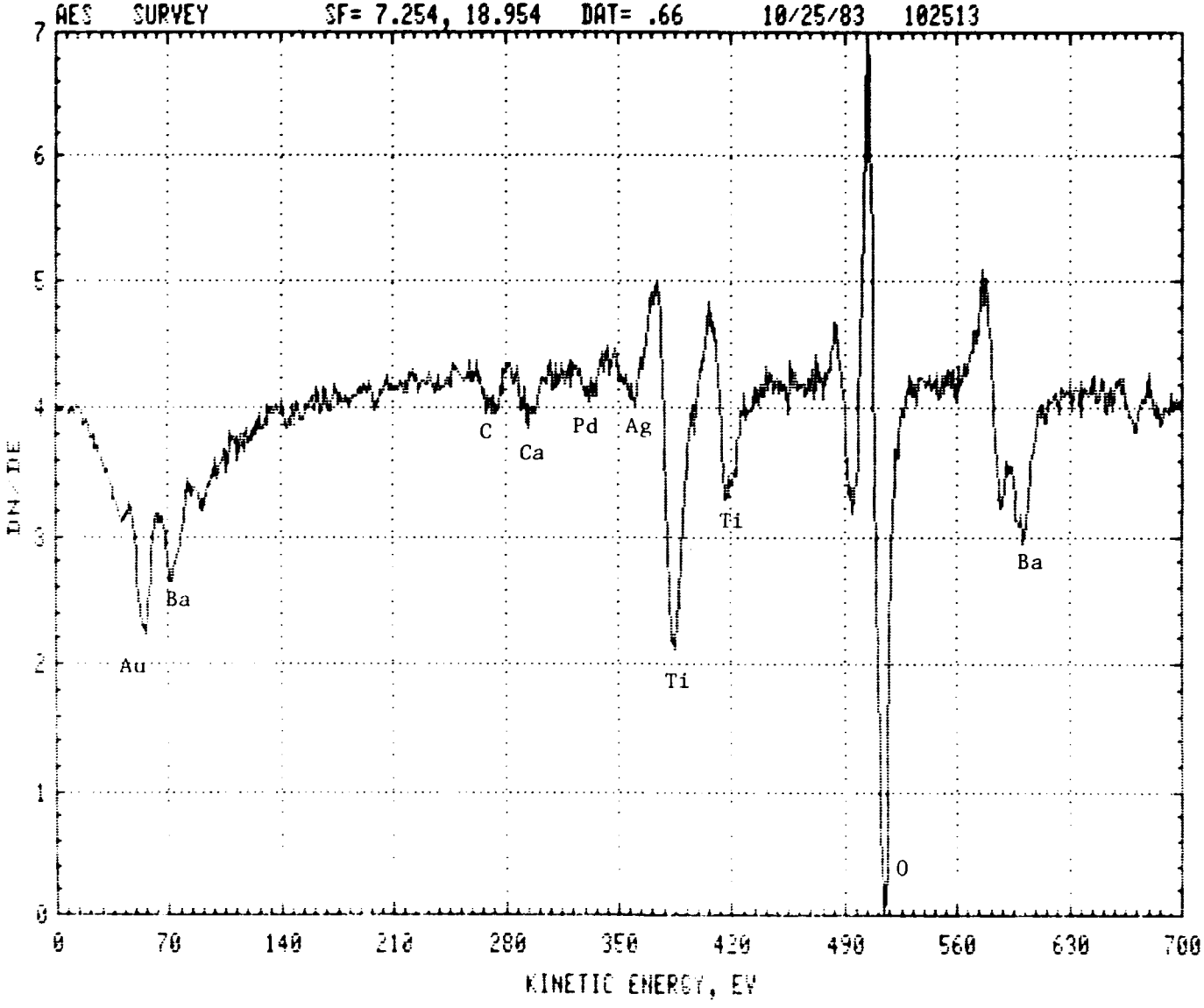

Figure 28a. Auger survey spectrum on degraded Z5U, near an electrode. (compare to Fig. 28b.)

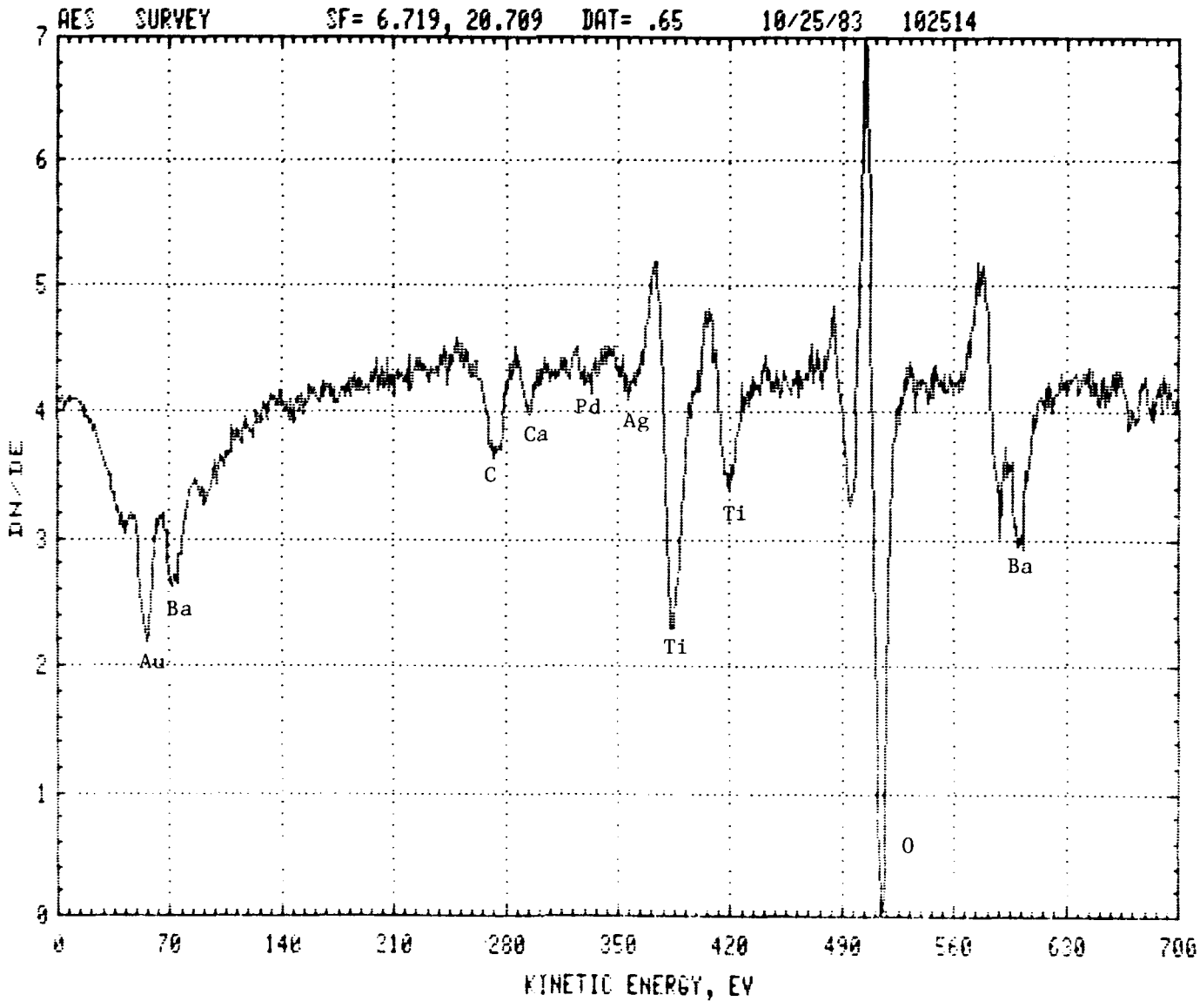

Figure 28b. Auger survey spectrum on degraded Z5U, halfway between electrodes. Many such spectra were taken on several degraded devices, and no oxygen (or other elemental) concentration gradient was evident.

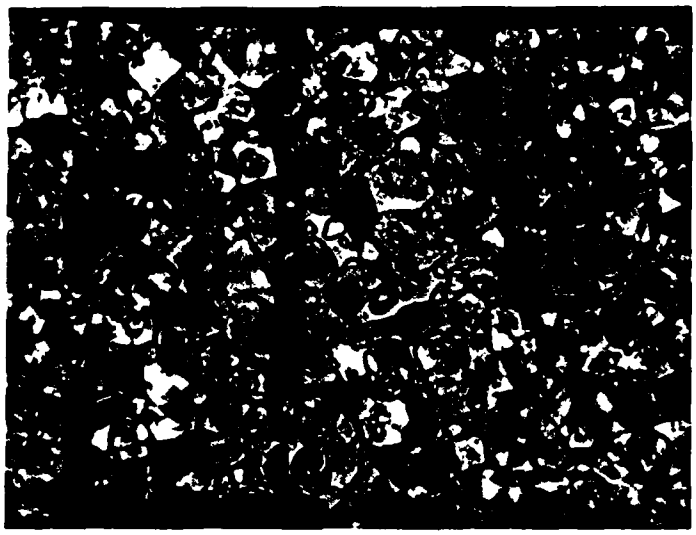

Figure 29. Apparent second phase region on Z5U from a second vendor (magnification - 630).

Figure 30a. SEM (5000X) of region similar to that in Figure 29.

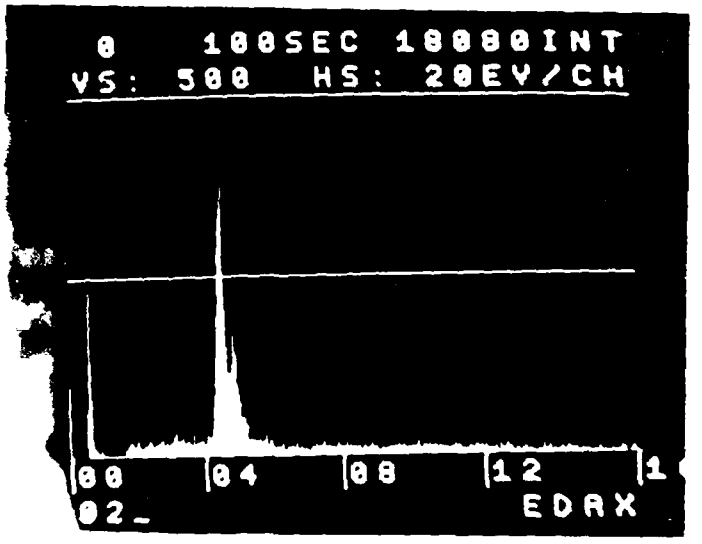

Figure 30b. EDAX spectrum in mid-grain region, showing Ba-Ti peaks (overlapped).

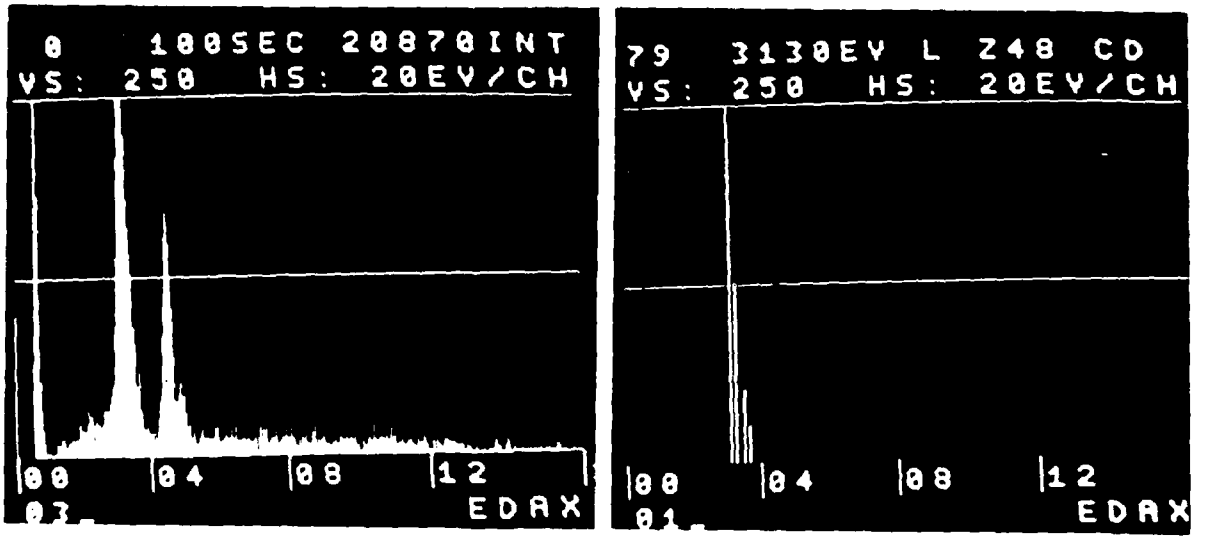

Figure 30c. EDAX spectrum in second phase region. Large peak to left of Ba/Ti peaks is identified as Cd (Cd markers are shown on right).

3.2 Electrode Defects

Electrodes are porous and of non-uniform thickness and separation. These features can have a potentially detrimental effect on reliability, due to enhanced electric field, as noted earlier in the I-V and 3/2 power model discussions. We noted in the latter discussion that enhanced electron emission would be expected from an electrode protuberance. On cross sectioned devices, electrode protuberances (large and small) seem fairly common, even in the limited number of capacitors we have polished. Examples of electrode "bulges" are shown below in Figure 31 for Z5U and X7R devices.

More serious are the narrower and longer protuberances such as that seen in Figure 32 for new X7R devices. These are the types of electrode defects at which electric field and leakage current will be strongly enhanced, even though these will also be increased for shorter, small tipped protuberances. In addition, if the tip of the protuberance extends into a void, the field and hence electron emission from the tip will be enhanced even further.

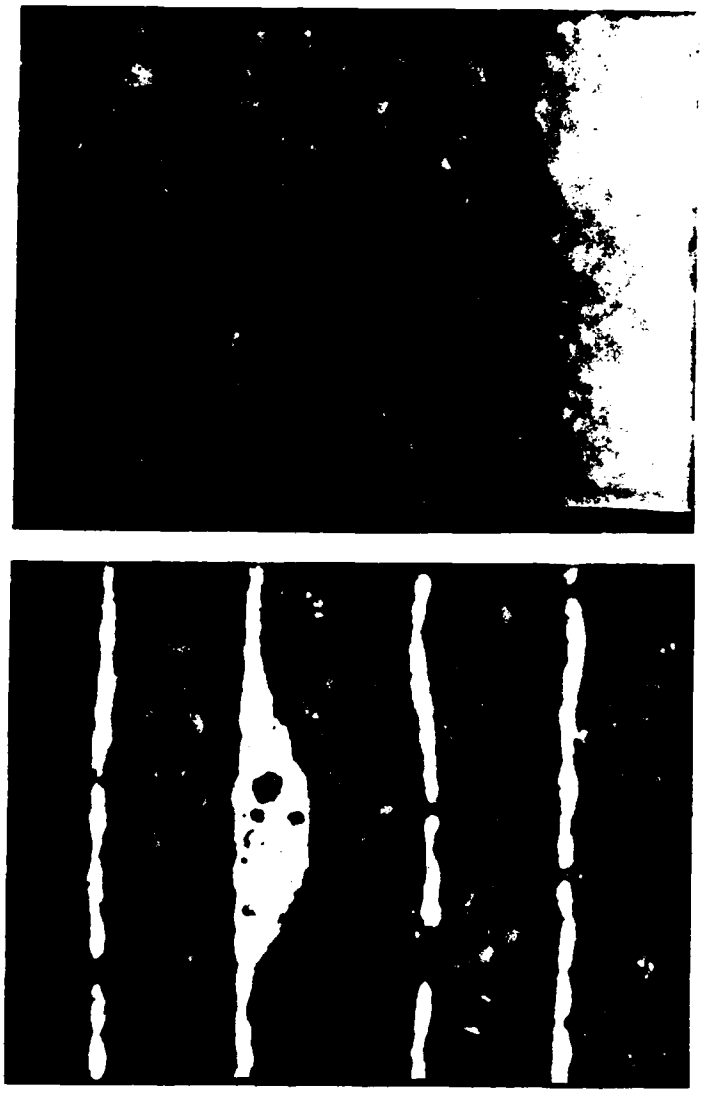

Figure 31. Electrode "bulges" for X7R (upper) and Z5U (lower) capacitors (400X).

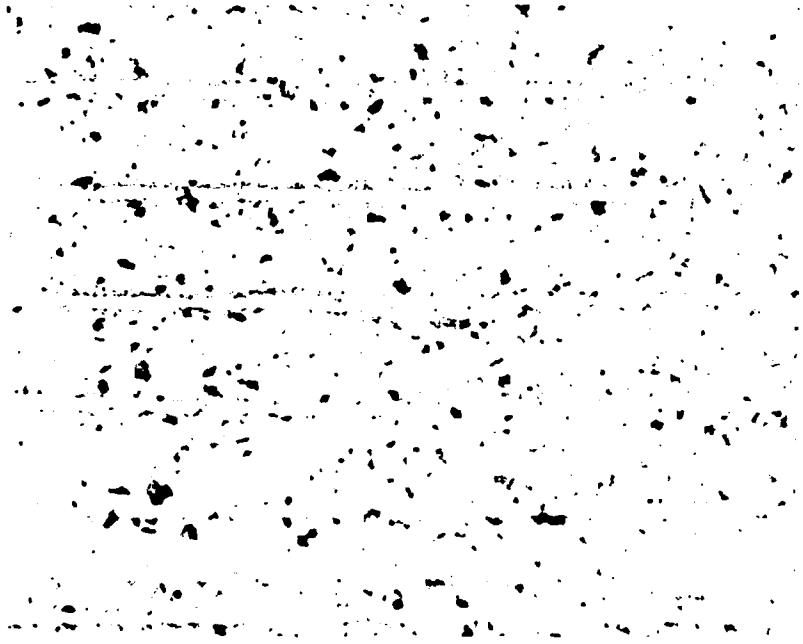

Figure 32. Electrode protuberances of two new X7R devices (Upper: 800X; lower: 500X).

4. THERMOELECTRIC MEASUREMENTS

Thermoelectric (TE) measurements were recently begun in order to separate carrier concentration and drift mobility for device ceramic, and to study their temperature dependence, for various degrees of reduction. Chips of X7R ceramic, fabricated similarly to MLC capacitors, but without the electrodes, are being measured.* Chip dimensions are 0.621 cm × 0.530 cm × 0.218 cm, and the TE voltage probes are placed on the larger faces, so that the electric field is in the same direction as it would be in the capacitor.

A schematic of the experimental arrangement is shown in Figure 33. The chip is mounted on a Cu block using Ag epoxy. Thermocouples to measure the top and bottom temperatures of the chip, and voltage leads, are also attached via Ag epoxy. The sample is placed in a temperature controlled tube furnace, and a temperature difference ΔT is established by the 10 watt heater in the Cu block. Output voltage (ΔV) is measured by a high input impedance electrometer (Keithly 610 C). The input impedance of the electrometer ($10^{14}\ \Omega$) is at least 100 times larger than the chip resistance as measured between the voltage probes. If this condition is not satisfied, the measurement circuit will load the crystal, and ΔV will be reduced. (For non-reduced chips, it is necessary to perform the measurements above room temperature to achieve this condition).

---

*Supplied by Corning Electronics, Raleigh, NC.

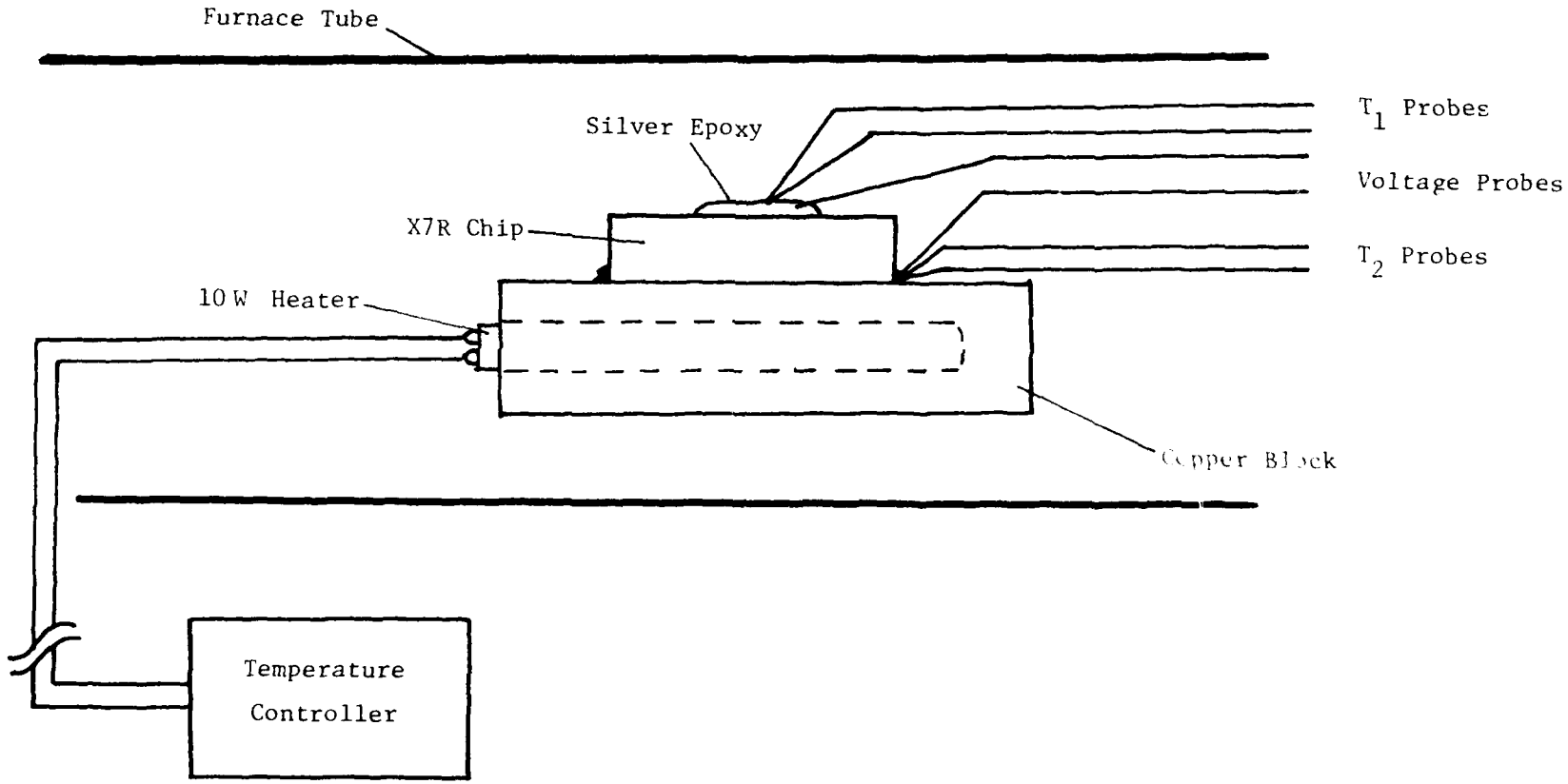

Figure 33. Setup for measuring thermoelectric coefficients. (Not to scale.)

Enough measurements have been made on two chips for some firm conclusions to be drawn (more extensive TE measurements are being continued on these and other chips). One of the chips is new (i.e. as received) and the other was reduced in forming gas ($10\%H_2/90\%N_2$) for 7 hours at 750°C.

The TE voltage ΔV is related to the temperature difference ΔT by the relation

$$\Delta V = S\Delta T \tag{8}$$

where S is the thermoelectric (Seebeck) coefficient. Results are shown in Figure 34 for the new sample (at 358°C) and the reduced sample (at 350°C). It is seen that the above linear relation is satisfied.

S values are shown versus temperature in Figure 35, where measurements were made on the new chip only above 200°C for reasons described earlier.

The flatness of the S vs T curves indicates that the carrier concentration is nearly independent of temperature. This is because the donor sources (oxygen vacancies, for example) are nearly completely ionized above room temperature, and the conductivity temperature dependence is attributable mainly to mobility.

Electrical conduction has been attributed to small polaron hopping for single crystal $BaTiO_3$[15], for reduced single crystals of $LiNbO_3$[16], for spinels[22] and wustite.[23] The concentration of polarons can be found from the expression for the thermoelectric coefficient[15,24]

$$S = \frac{k}{q} \ell n \frac{N}{n} \tag{9}$$

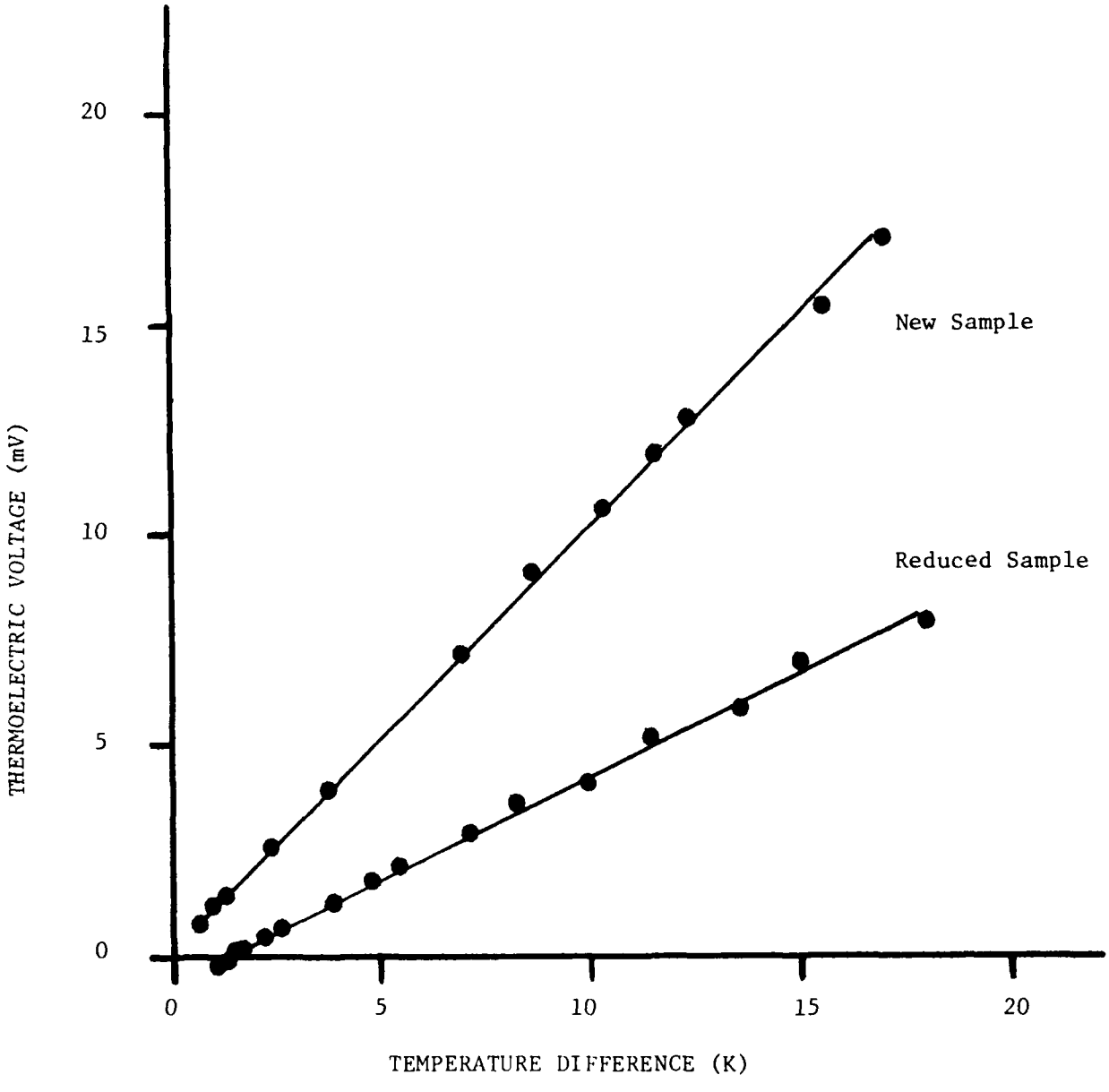

Figure 34. Thermoelectric voltage versus temperature difference for new and reduced X7R ceramic samples.

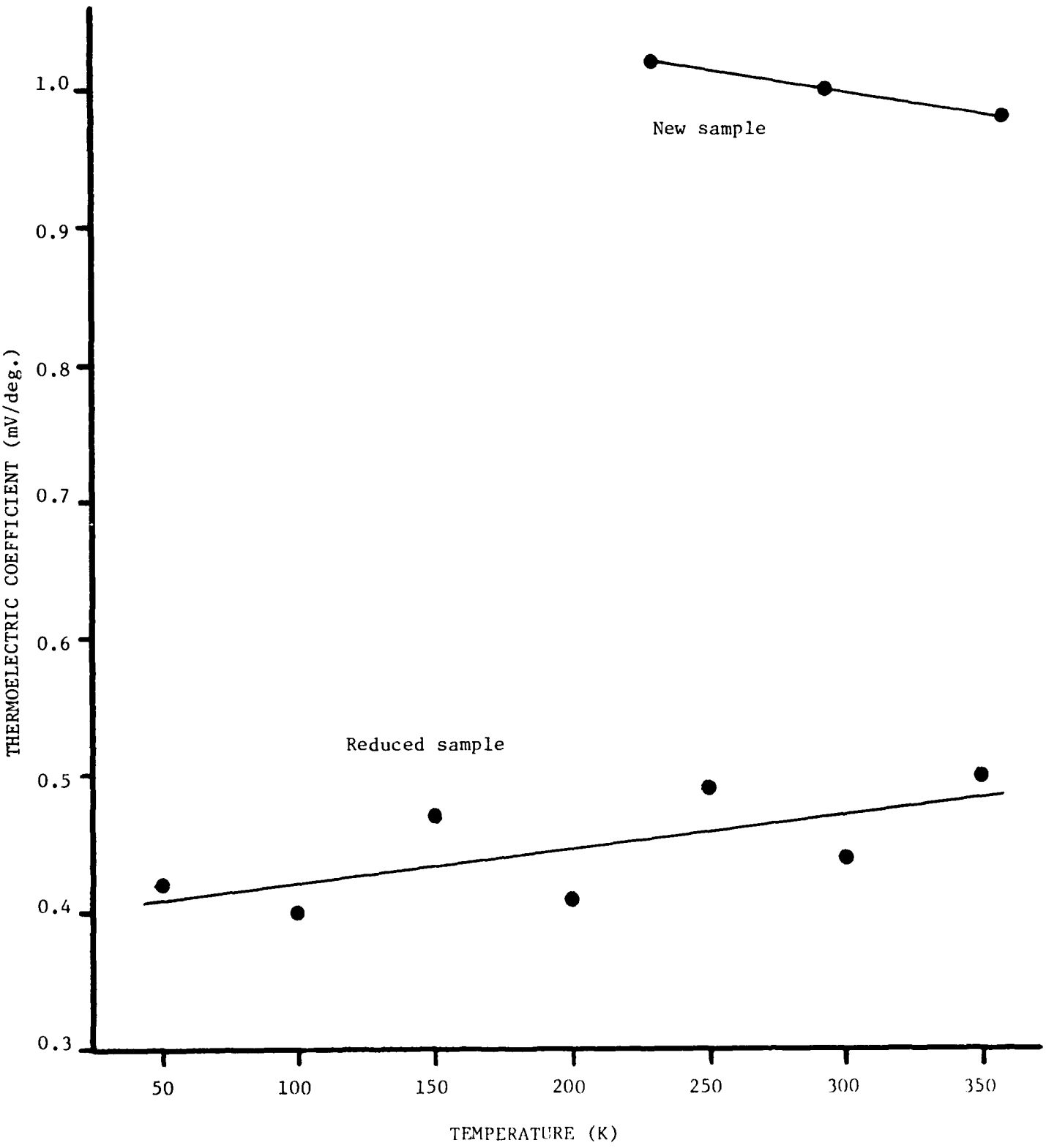

Figure 35. Thermoelectric coefficient versus temperature for new and reduced X7R ceramic.

where $k/q = 8.63 \times 10^{-2}$ mV/K

n = polaron concentration

N = hopping site density

If we assume that the hopping site is the Ti^{+} ion, then $N = 1.56 \times 10^{22}\ cm^{-3}$, and n is determined from relation (9) above. These values are shown versus inverse temperature for the two samples in Figure 36. The reduced sample has essentially constant carrier concentration of $\approx 10^{20}\ cm^{-3}$, with the new sample having a weak temperature variation, with $n \approx 3 \times 10^{16}\ cm^{-3}$ at room temperature (extrapolated).

The drift mobilities for these two samples were determined by simultaneously measuring electrical conductivity σ, and solving for μ from the relation

$$\sigma = q\, n\, \mu \qquad (10)$$

Mobility values are shown versus inverse temperature in Figure 37. Such linear characteristics are anticipated for small polaron hopping.

Thermal activation energies for carrier concentration (ϕ_n), mobility (ϕ_μ) and conductivity (ϕ) are shown in Table 1.

Table 1

Thermal Activation Energies (eV)

Sample	Carrier Concentration	Mobility	Conductivity
New	0.19	1.03	1.22
Reduced	~ 0	0.34	0.34

Even though these results are only preliminary, several points appear to be established for new and reduced non-electroded X7R ceramic:

1. Thermoelectric voltages were negative and stable in all cases, indicating that the charge carrier is the electron;

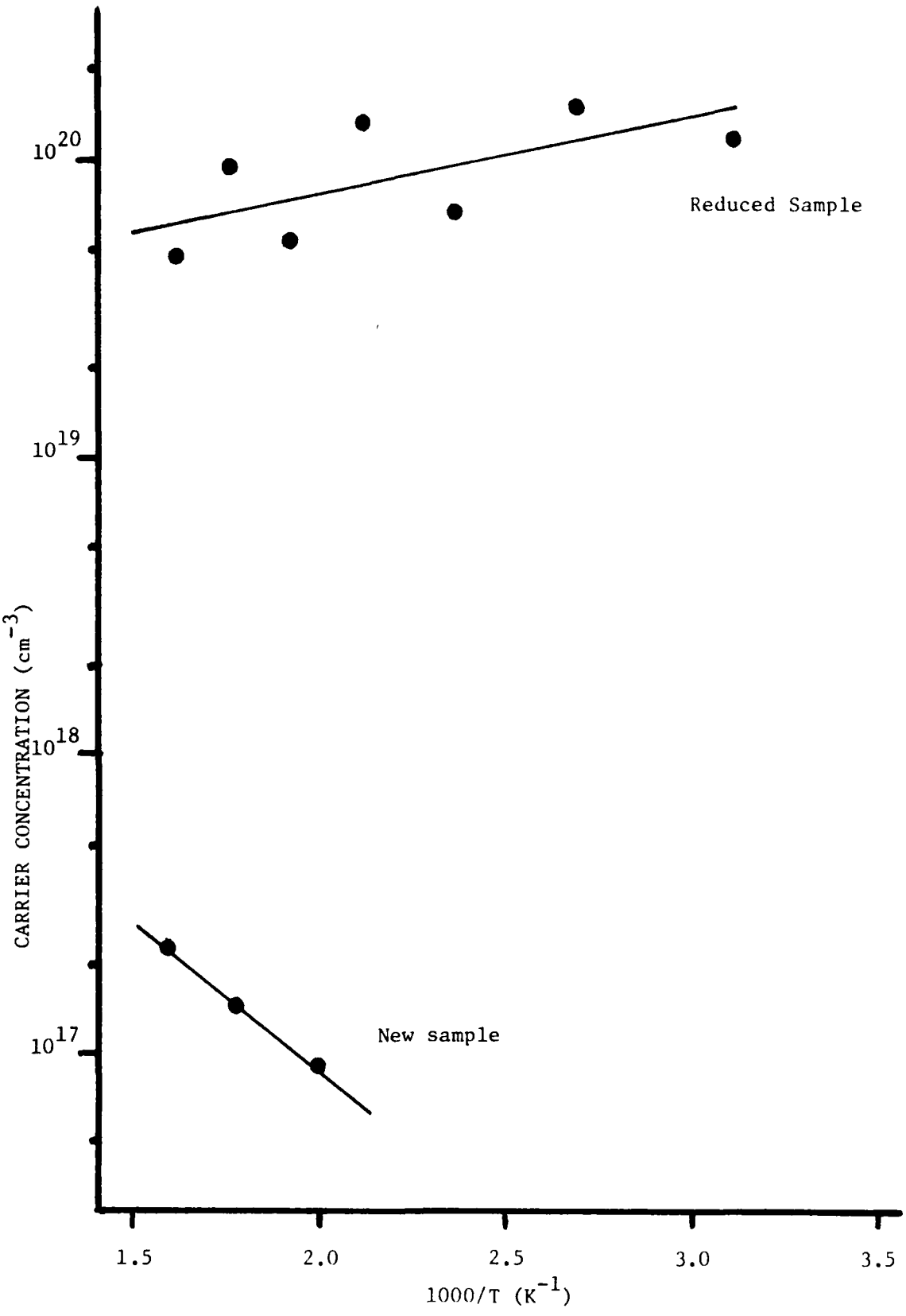

Figure 36. Carrier concentration versus inverse temperature for new and reduced X7R ceramic.

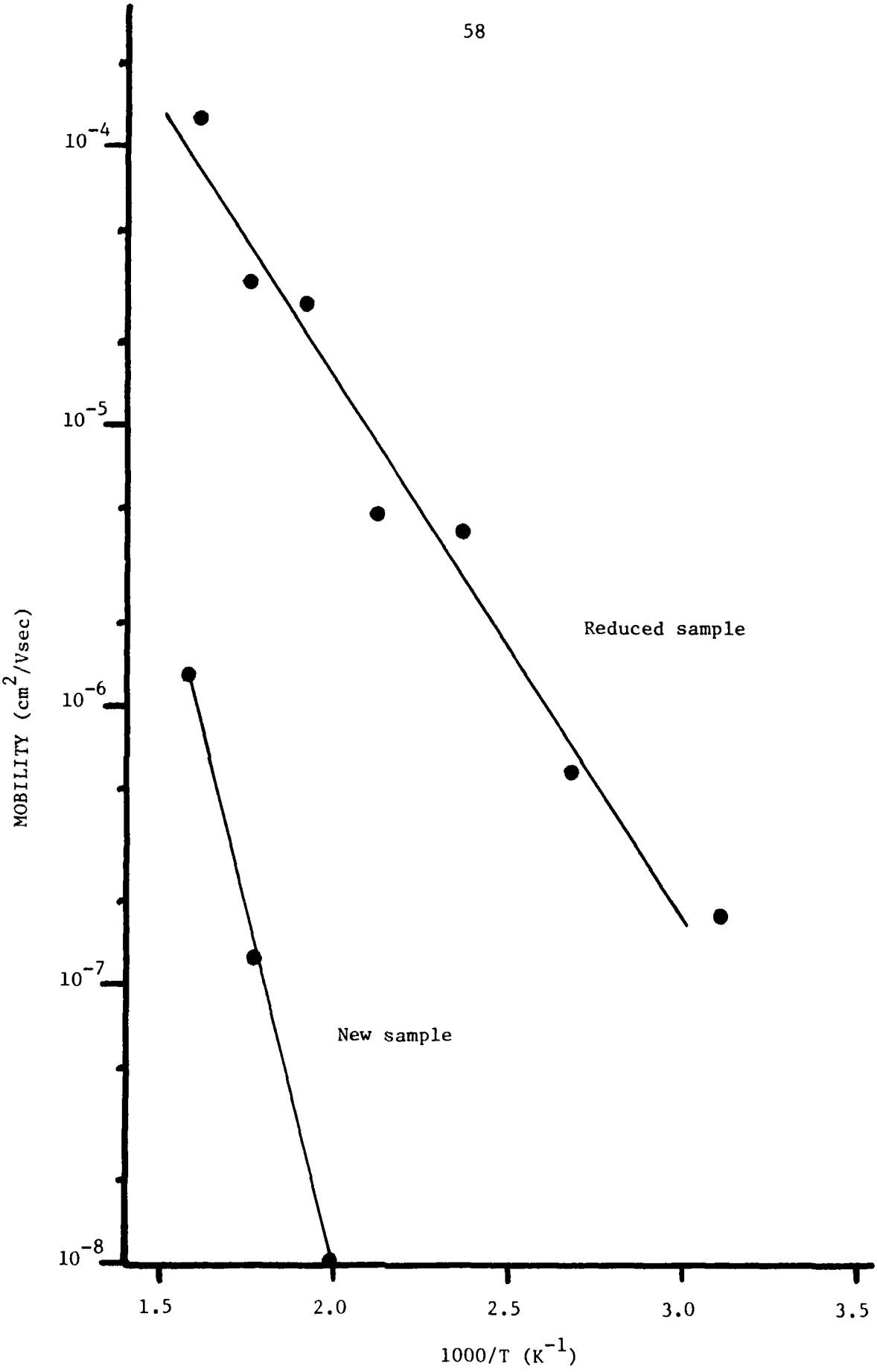

Figure 37. Drift mobility versus inverse temperature for new and reduced X7R ceramic.

2. The weak temperature dependence of the carrier concentration indicates near-complete ionization of donors;

3. Conductivity activation energy is ~ 1.2eV for the new chip, which is close to that of a new X7R capacitor (1.2 - 1.3eV);

4. The decrease in activation energy for the conductivity of the reduced chip (0.34eV) is attributed largely to mobility. This decrease parallels that seen in degraded capacitors.

These results, however, are uncertain to the following extent:

1. A constant hopping center concentration (equal to the Ti^{+} ion concentration in $BaTiO_3$) was assumed. X7R ceramic is not totally $BaTiO_3$, and it is not clear that the only (or even the major) hopping site is the Ti^{+} ion. The hopping site concentration may change with reduction of the ceramic. We have not been able to take that into account. We hope to clarify this point by determining the carrier concentration on these and other samples using Hall effect measurements.

2. There is some concern about the uniformity of the reduced sample. This will be checked by cross sectioning, and appropriate steps taken if necessary (such as post-reduction annealing in Ar) to homogenize future samples.

5. OTHER STUDIES

5.1 Impedance Dispersion

Impedance measurements were made on several new and degraded devices. Capacitance, dissipation factor (D), and conductance (G) were measured as functions of frequency, for devices with insulation resistances greater than about 1 MΩ. If grain boundary space charge or domain walls change substantially, these could be expected to show up in the dispersion characteristics of the above parameters. Such measurements, utilizing complex plane plots (similar to Cole-Cole plots) have been used to study grain boundary effects in PTC $BaTiO_3$ ceramic[25], in ferroelectric $Pb_5Ge_3O_{11}$[26] and a variety of other ceramic materials (such as ZnO, Al_2O_3, zirconates etc.).

For our samples, no major differences were seen in the dispersion characteristics over the 10 Hz - 10 MHz frequency range. The normal fall in C and increase in D with frequency up to the resonant frequency for the capacitance value being measured were seen in all cases. An example is seen in Figure 38, for C values. Even though G values were larger at lower frequencies (as expected due to DC shunt) no anomalous dispersive characteristics were evident. This leads to several comments about the grain boundary space charge/barrier height for these devices: either i) the space charge is not large enough to be significant, or ii) it doesn't change significantly (which would be surprising if the bulk resistivity decreased by several orders of magnitude), or iii) any changes are less than the detection limits of our impedance measurements.

This absence of change in dispersion characteristics following degradation, combined with the similarities of our SCLC and thermoelectric results to those reported for $BaTiO_3$ single crystal, seem to indicate that

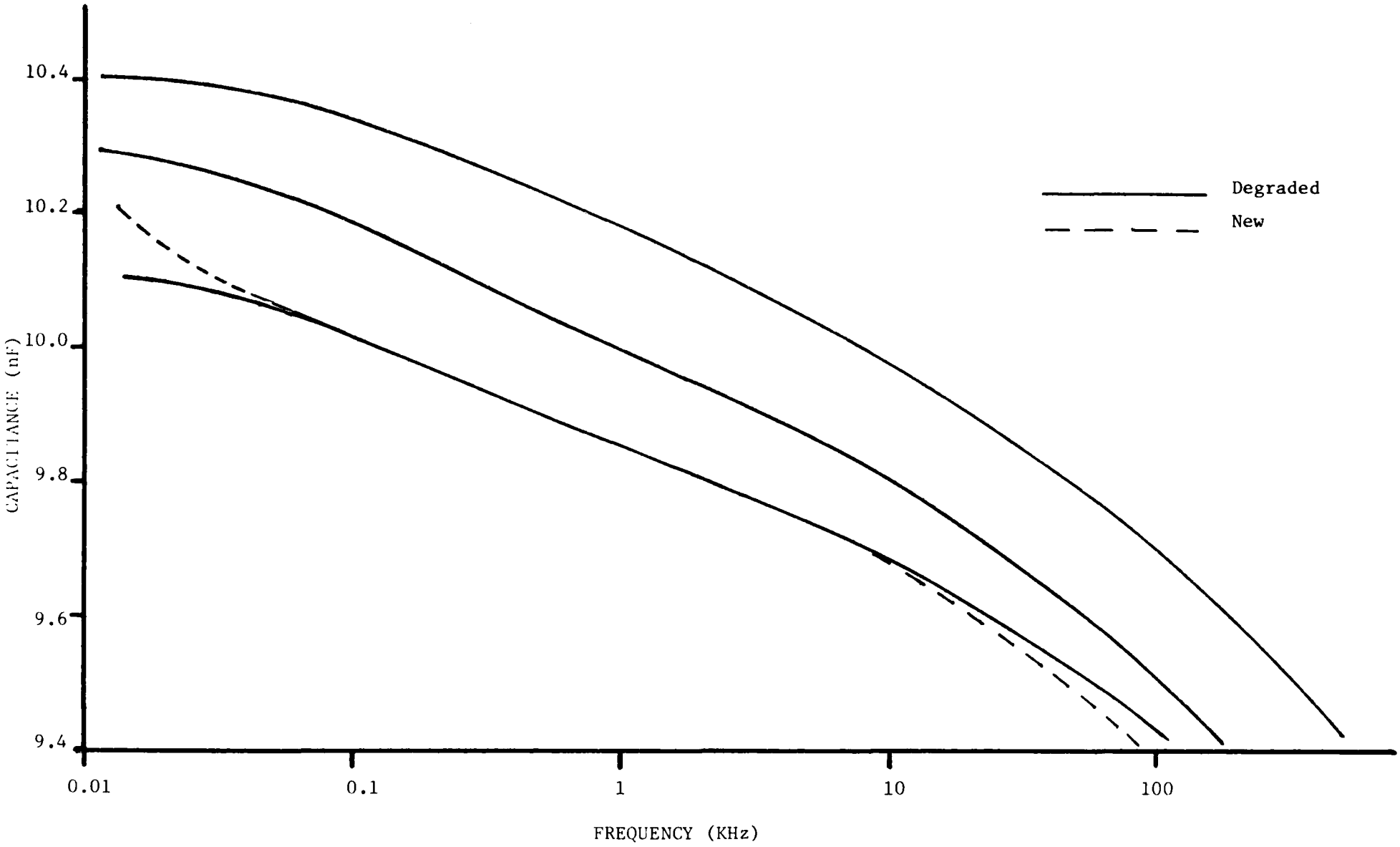

Figure 38. Capacitance versus frequency for three degraded and one new X7R devices. The degraded devices have insulation resistances less than 10^8 ohm.

the grain boundary does not play a dominant role with respect to leakage current directly, even though ionic diffusion may be larger along grain boundaries.

5.2 Photoconductivity

Photoconductivity measurements were attempted on polished devices, in an effort to deduce electron lifetime and mobility. However, these measurements failed to be productive, and are being replaced by the vander Pauw method of Hall effect measurements.

Using 1 μsec pulses from a Xenon flash lamp, the change in conductivity was barely detectable. (Steady state illumination causes sample temperature to rise, which in turn causes a dC/dT current, under bias.) Sample conductivity was monitored by displaying the flashlamp output and circuit current (through a standard resistor) simultaneously on a dual trace oscilloscope.

It is felt that the photoconductivity is being swamped out by leakage currents that exist at the polished capacitor surface. Enhanced DC conduction in this region was detected by light emission from certain regions of the polished face when a voltage was applied across the electrodes, under microscope observation. This is seen in Figure 39 for applied voltages of zero and 200 volts. Localized conduction is occuring in certain regions, causing photon emission by heating or luminescence.

Our recent success with thermoelectric measurements indicates that Hall measurements can also be done on non-electroded samples. Carrier concentration and mobility information derived from Hall measurements will complement the TE information, and help to establish conclusively whether or not electron transfer occurs by means of small polaron hopping.[16]

6. FUTURE WORK

Our most immediate tasks are the following:

1. To complete thermoelectric studies on a larger number of reduced samples; to verify the uniformity of such samples over a resistivity range as large as possible.

2. To perform Hall effect studies on a similar set of non-electroded samples, using the 4-lead vander Pauw technique; specially made samples of $\simeq 0.5$ mm thickness will be used here.

3. To continue I-V analysis and modelling on new and degraded devices.

REFERENCES

[1] "The Reliability of Multilayer Ceramic Capacitors" Publication NMAB-400, National Academy of Sciences, Washington, DC (1983).

[2] Eugene Loh, "A Model of DC Leakage in Ceramic Capacitors, J. Appl. Phys. 53, 6229 (1982).

[3] C. Schaffrin, "Oxygen Diffusion in $BaTiO_3$ Ceramic", Phys. Stat. Sol. (a), 35, 79 (1976).

[4] William J. Minford, "Accelerated Life Testing and Reliability of High K Multilayer Ceramic Capacitors", IEEE Trans. Components, Hybrids and Manuf. Tech., CHMT-5, 297 (1982).

[5] Y. Y. Sabara, A. Y. Kudzin and K. A. Kolesnichenko, "Space Charge Limited Currents in Barium Titanate Single Crystals", Phys. Stat. Sol. (a) 38, K131 (1976).

[6] L. Benguigi, "Space Charge Limited Currents in $BaTiO_3$ Single Crystals", Sol. St. Commun. 7, 1245 (1969).

[7] R. T. Thomas, "Time Dependence of the Electrical Conductivity of $BaTiO_3$ Single Crystals Heated in Oxygen", J. Phys. D: Appl. Phys., 3, 1434 (1970).

[8] D. D. Glower and R. C. Heckman, "Conduction-Ionic or Electronic-in $BaTiO_3$", J. Chem. Phys. 41, 877 (1964).

[9] R. Stumpe, D. Wagner and D. Bauerle, "Influence of Bulk and Interface Properties on the Electric Transport in ABO_3 Perovskites", Phys. Stat. Sol. (a) 75, 143 (1983).

[10] S. A. Long and R. N. Blumenthal, "Ti-Rich Nonstoichiometric $BaTiO_3$: I, High-Temperature Electrical Conductivity Measurements", J. Amer. Ceram. Soc. 54, 515 (1971).

[11] N. H. Chan, R. K. Sharma and D. M. Smyth, "Nonstoichiometry in Acceptor-Doped $BaTiO_3$", J. Amer. Ceram. Soc. 65, 167 (1982).

[12] Jeffrey D. Keck, "Electrical Degradation in High Purity Barium Titanate", Ph.D. Thesis, Univ. of Missouri-Rolla, 1976.

[13] L. Benguigi, "Electrical Phenomena in Barium Titanate Ceramics", J. Phys. Chem. Sol. 34, 573 (1973).

[14] W. A. Schultze, L. E. Cross, and W. R. Buessem, "Degradation of $BaTiO_3$ Ceramic Under High ac Electric Field", J. Amer. Ceram. Soc. 63, 83 (1980).

[15] D. L. Ridpath and D. A. Wright, "Electrical Conductivity of Reduced Barium Titanate Crystals", J. Mater, Sci. 5, 487 (1970).

[16] P. Nagels, "Experimental Hall Effect Data for a Small-Polaron Semiconductor", from The Hall Effect and Its Applications (C. L. Chien and C. R. Westgate, ed.), Plenum Press (1980).

[17] M. A. Lampert and P. Mark, Current Injection in Solids, Academic

[18] M. A. Lampert and R. B. Schilling, "Current Injection in Solids: The Regional Approximation Method"; Ch. 1 in Semiconductors and Semimetals, Vol. 6 (ed. by R. K. Willardson and A. C. Beer), Academic Press (1970).

[19] S. M. Sze, Physics of Semiconductor Devices (2nd Ed.), John Wiley and Sons (1981).

[20] B. C. Eu and A. S. Wagh, "Nonlinear Field Dependence of Carrier Mobilities and Irreversible Thermodynamics in Semiconductors", Phys. Rev. B. 27, 1037 (1983).

[21] J. B. Gunn, "Instabilities of Current in III-V Semiconductors", IBM Jour. 141 (April 1964).

[22] T. O. Mason and H. K. Bowen, "Electronic Conduction and Thermopower of Magnetite and Iron-Aluminate Spinels", J. Amer. Ceram. Soc. 64, 237 (1981).

[23] J. D. Hodge and H. K. Bowen, "Measurement of Low-Temperature Thermoelectric Power for Quenched Wustite", J. Amer. Ceram. Soc. 64, 220 (1981).

[24] Klaus-Dieter Schotte, "The Thermoelectric Properties of the Small Polaron", Zeit. fur Physik 196, 393 (1966).

[25] H. Nemoto and I. Oda, "Direct Examination of PTC Action of Single Grain Boundaries in Semiconducting $BaTiO_3$ Ceramics", J. Amer. Ceram. Soc. 63, 398 (1980).

[26] L. E. Cross and T. W. Cline, "Contributions to the Dielectric Response from Charged Domain Walls in Ferroelectric $Pb_5Ge_3O_{11}$", Ferroelectrics 11, 333 (1976).

Appendix I

A. Participants

1. Dr. L. C. Burton - Professor of Electrical Engineering and Materials Engineering; Principal Investigator

2. Dr. K. C. Lee - Visiting Scholar from Ulsan Technical Institute, Ulsan, South Korea

3. H. Y. Lee - Ph.D. candidate in Materials Engineering Science

4. N. Schunke - Masters candidate in Materials Engineering

5. J. Henry - EE student

6. K. Boggs - EE student

7. I. Sharif - EE student

B. Reports and Papers Related to this Program.

1. "Intrinsic Mechanisms of Multi-Layer-Ceramic Capacitor Failure", report presented at the Center for Dielectric Studies Meeting, Penn State University, Nov. 8, 1983. (Summary of this report sent to Dr. J. Biggers, MRL, Nov. 30, 1983).

2. "End-of-the-Fiscal Year" letter submitted to Dr. C. T. Lynch, ONR, Nov. 21, 1983.

3. "Models for Leakage Currents in Multi-Layer Ceramic Capacitors" paper to be presented at 86th Annual Meeting of the American Ceramic Society, Pittsburgh, 4/29-5/3/84.

4. "Leakage Currents in Degraded Multi-Layer Ceramic Capacitors" paper to be presented at 34th Electronic Components Conference, New Orleans, 5/14-5/16/84 (sent to ONR as Technical Report).

5. "Electrical Characterization of Ceramics and Polymers" paper to be presented at the Advances in Materials Characterization Conference, Alfred College, Alfred, NY, 8/1-8/3/84.

Appendix II

"Leakage Currents in Degraded Multi-Layer Ceramic Capacitors" — paper to be presented at Electronic Components Conference, New Orleans, May 11-14, 1984.

LEAKAGE CURRENTS IN DEGRADED MULTI-LAYER CERAMIC CAPACITORS

by

Larry C. Burton
Departments of Electrical Engineering and Materials Engineering
Virginia Polytechnic Institute and State University
Blacksburg, VA 24061

Abstract

Leakage currents in new and degraded X7R type multi-layer ceramic capacitors show both ohmic and space charge limited behavior. The near-3/2 power voltage characteristic ($I\alpha V^{3/2}$) of new devices can be attributed to electron emission from electrode points. The quadratic behavior ($I\alpha V^2$) for moderately degraded devices represents space charge limited emission from planar electrodes. This emission may evolve from the point emission due to resistivity decreases that occur in the emission region as a result of ion movement. For these currents, electrons are believed to be the dominant charge carriers. Neither Schottky nor Poole-Frenkel currents were identified. Thermal activation energies were found to decrease from $\sim$ 1.3 eV for new devices, to zero for degraded ones, corresponding to resistivity decreases from $\sim 10^{13}$ Ω-cm (at 125°C) to 10^5 Ω-cm or less. Drift mobility increase (along with that of carrier concentration) may be an important factor in leakage current increase during degradation.

I. Introduction

It is known that degradation of insulation resistance, as contrasted to shifts in capacitance or dissipation factor, is the primary failure concern for high dielectric constant multi-layer ceramic (MLC) capacitors.[1,2] It is, however, not easy to measure the true DC leakage current for a good MLC device at room temperature due to the presence of additional currents that exist after a capacitor is charged, such as polarization and pyroelectric currents. The sum of these currents is usually larger than the DC leakage current over a period of many hours. It is not difficult, however, to measure steady state leakage at elevated temperatures, above roughly 100°C. This is because the DC resistivity is decreased, and the other current types decay faster.

DC leakage currents in new MLC devices of more or less standard composition (X7R for example) are probably due to the same mechanisms. When similar devices (X7Rs of different values) are degraded under the same conditions, similar trends are seen, both during degradation and in subsequently measured electrical characteristics.

The dominant leakage current charge carrier, and its mode of transport, have not been established. The current has been attributed, in MLC capacitors, to Poole-Frenkel emission[3], and indirectly (through the 1.19 eV activation energy) to oxygen vacancy diffusion.[1,4]

Numerous conductivity studies have been reported for $BaTiO_3$ ceramic[5-10] and single crystal[11-14] material. For the ceramic, electron (n-type) conduction seems predominant[5,6], with the conductivity strongly affected by impurities[7,8]. Space charge limited[8,9,11,12] and Schottky[10] currents have been reported. For the single crystal case, space charge limited currents[11,12] double injection[13], both ionic and electronic carriers in different temperature ranges[14] and small polaron hopping[15] have been reported. Some of these $BaTiO_3$ ceramic and single crystal studies may pertain to the various types of ceramic used in MLC capacitors.

Thus, there are several questions related to MLC capacitor leakage current that should be addressed. Some of these are:

1. What is the dominant charge carrier? Does it change (from say ionic to electronic) at some point during capacitor degradation?

2. What are the sources of the carriers (oxygen vacancies, electrodes, etc.)?

3. What is the mode of carrier transport (hopping, grain boundary tunneling, etc.) and does it also change with time?

4. What role does carrier transport play in degradation, as contrasted to carrier concentration?

These questions are addressed later in varying degrees. Before they are considered further, the types of current that might be expected to flow in MLC devices are reviewed.

II. Current Types

Ohmic

This can consist of both electronic (electron and/or hole) and ionic contributions. The voltage (V) dependence of current (I) is expressed as

$$I = qA\, n\mu\, V/L \qquad (1)$$

where q = electronic charge
A,L = cross sectional area and thickness
n = carrier density
μ = carrier drift mobility

The temperature dependence of I is contained in n and/or μ, and may be expressed in terms of an activation energy φ:

$$I = I_o e^{-\phi/kT} \qquad (2)$$

Space Charge Limited Current (SCLC): Planar Electrodes

In this case, electron (or hole) density injected from the electrodes exceeds the native bulk carrier concentration. This current applies to electronic carriers, since ions aren't expected to be injected from the electrodes in MLC devices. For planar electrodes, which might approximate MLC electrodes, a current-voltage relation is[16]

$$I = \frac{9}{8} A\, \theta\, \varepsilon\mu\, V^2/L^3 \qquad (3)$$

where ε = permitivity and θ is a trapping parameter defined by

$$\theta = \frac{N_c}{2N_t}\, e^{-\Delta E/kT} \qquad (4)$$

where N_c = conduction band density of states and N_t = shallow trap density, located at energy ΔE below the conduction band edge.

These relations can be used to estimate μ, N_t and ΔE if the SCL characteristic defined by equation 3 is

measured.

SCLS: Spherical (Point) Electrode

Current from a hemispherical point cathode emitting toward an anode of much larger radius can be described by the following I-V relation:[17]

$$I = \frac{2\pi\sqrt{2}}{3} \mu(\theta q \epsilon n)^{\frac{1}{2}} V^{3/2} \quad (5)$$

where all of the parameters were previously defined.

SEM pictures indicate the irregular nature of MLC electrodes. If SCLC is present, a non-planar electrode model such as that above may be necessary.

SCLC Variations

The two types of SCLC noted above are for specified electrode geometries and a discrete shallow trap. In reality, traps are unlikely to be discrete in a ceramic, and will probably be distributed across an energy range. Such extended trap distributions, in addition to the possible existence of diffusion currents (which were neglected above) modify the current-voltage dependence, usually towards a voltage exponent greater than two. Details are described in the literature.[16,17]

Schottky Current (Poole-Frenkel in bulk)

In this case, electron or hole currents increase due to lowering of a potential barrier by an external voltage, at the electrode (Schottky effect), or at a trap or grain boundary in the bulk (Poole-Frenkel effect).

The current-voltage relation for both of these currents has the form[18]

$$I = I_o \exp\left[\frac{B}{T}(E/K)^{\frac{1}{2}}\right] \quad (6)$$

where B is constant, E is electric field, K is dielectric constant and T is temperature.

The Schottky effect only occurs at a rectifying contact, and probably doesn't apply to MLC capacitors. Bulk effects are more likely, due to electrons located in potential wells at traps and grain boundaries.

Field Dependent Factors

The dielectric constant appears in all of the above relations except the ohmic one. Voltage and temperature dependence of this factor must be included in these relations, and is more significant for Z5U material than for X7R.

Field dependent mobility could alter the I-V characteristics. This effect has been reported for a variety of single crystal semiconductors[19,20], and in these cases becomes predominant at low temperatures (< 300K). It is unlikely that it is a factor in polycrystalline ceramic above room temperature.

At high fields, the bulk carrier concentration can be increased due to avalanche effects. This is probably not a factor well below the breakdown strength of the dielectric, although it might be significant in localized regions of higher fields (caused by electrode non-uniformity, for example).

Other Factors

Additional current mechanisms, which are sometimes controlling factors in other structures, are probably not important for MLC devices. These include tunneling, surface leakage and field-induced exoemission.[21] Even though tunneling is important in other semiconductor devices,[22] and could potentially occur in MLC capacitors in high field locations (such as grain boundaries), we have seen no indication of it in I-V curves. Surface leakage and exoemission are probably not factors here because the electroded regions of these devices are buried in ceramic. Even though these external ceramic regions might serve as a local source of oxygen, they probably don't play an active part in current transport. External leakage paths on the package surface are not of concern to us here.

That a combination of the above currents may exist simultaneously, with particular ones dominant over specific voltage and temperature ranges, and that both electronic and ionic carriers may contribute, should be kept in mind during modelling of leakage currents for these devices. Also important is the high probability that leakage currents increase during lifetests in localized regions,[23] which may account for some of the variability seen in the I-V characteristics.

III. Experimental Techniques

Most of the measurements were made on 10nF and 1μF X7R devices, both in the new and degraded states. Some were obtained from commercial vendors following accelerated lifetests (nominally at 125°C, twice rated voltage), and we degraded additional capacitors of the same types (typically at 180°, four or eight times rated voltage). It was not our objective to perform statistical lifetest studies, but to ascertain and model trends that were common in the leakage current behavior of devices aged under the above conditions. The types of behavior discussed below were similar for 10nF and 1μF devices, for both sets of accelerating conditions.

Current-voltage measurements were made using a Hewlett-Packard 6116A voltage supply and a Keithley 610B electrometer. Sample temperature could be maintained to within about ± 0.2°C, from room temperature to 200°C.

Current decay or instability was a problem in several instances. a) For new devices, very long time constants for current stabilization were seen near room temperature. For this reason, measurements were made on these devices in the 100-200°C range. b) Degraded devices exhibiting space charge behavior are inherently unstable in voltage regions of trap filling and emptying. In this region, average values were recorded, until the region was traversed and the currents became stable. c) Some degraded devices exhibited unstable behavior over the entire voltage range, and self-healing effects (suddent decreases in current by up to several orders of magnitude) were often seen in these cases. d) An unstable increase was seen as current exceeded the 10^{-4} to 10^{-3} amp range, probably caused by localized heating in the device. Since only DC voltages were used, currents were kept below about 10^{-4} A.

Time dependent characteristics such as those mentioned above are not further considered, unless it is felt that they were due to trap filling effects. (For example, as shallow traps fill, current increases rapidly with voltage due to the large mobility increase).

Capacitance and dissipation factor were measured for new and degraded devices from 10 Hz to 13 MHz on a Hewlett-Packard 4192A Impedance Analyzer, in order

to ascertain if any significant changes are occurring in these parameters. Except in the extreme cases (insulation resistance less than a few KΩ), no major changes were seen. This seems to indicate that any changes occurring at grain boundaries, interfaces etc. are not significant enough to show up. These measurements, therefore, aren't discussed further below.

It should also be noted that early in the program, Z5U capacitors also showed SCL and ohmic behavior similar to that of the X7Rs. Tests on Z5Us were discontinued due to the large dependence of interpretation on their more variable dielectric constant, and to the fact that X7R devices are more relevant to higher reliability needs. Therefore, only X7R measurements are discussed below.

IV. Results and Discussion

Results

I-V curves for new 10nF and 1μF X7R devices are shown in Figure 1 (T = 170°C). The near 3/2 power dependence ($I \alpha V^{3/2}$), especially at higher voltages, is typical of new devices.

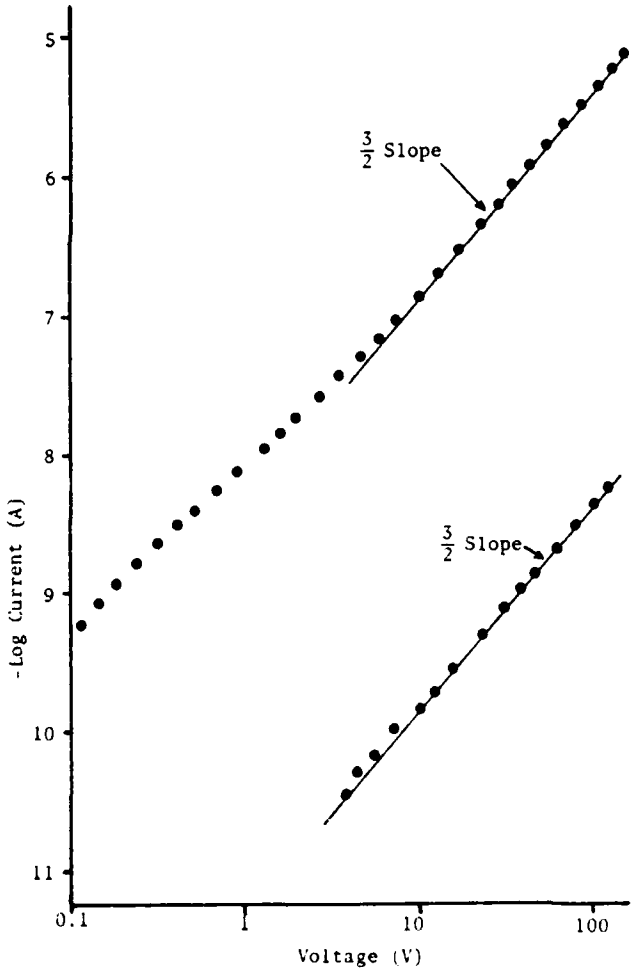

Figure 1. I-V curves for new 10nF (lower) and 1μF (upper) X7R devices.

Degraded devices show a variety of characteristics. The most commonly seen stable characteristics are: ohmic behavior at low voltages ($\lesssim$ 1 volt); SCLC square law or near square law behavior ($I \alpha V^2$) at higher voltages ($1 \lesssim V \lesssim 100$ v); a steep region on the I-V characteristic which is probably attributable to trap filling; ohmic behavior for severely degraded devices over the entire voltage range. Three device characteristics are shown in Figure 2, where the most degraded device is ohmic, the other two exhibiting SCLC characteristics.

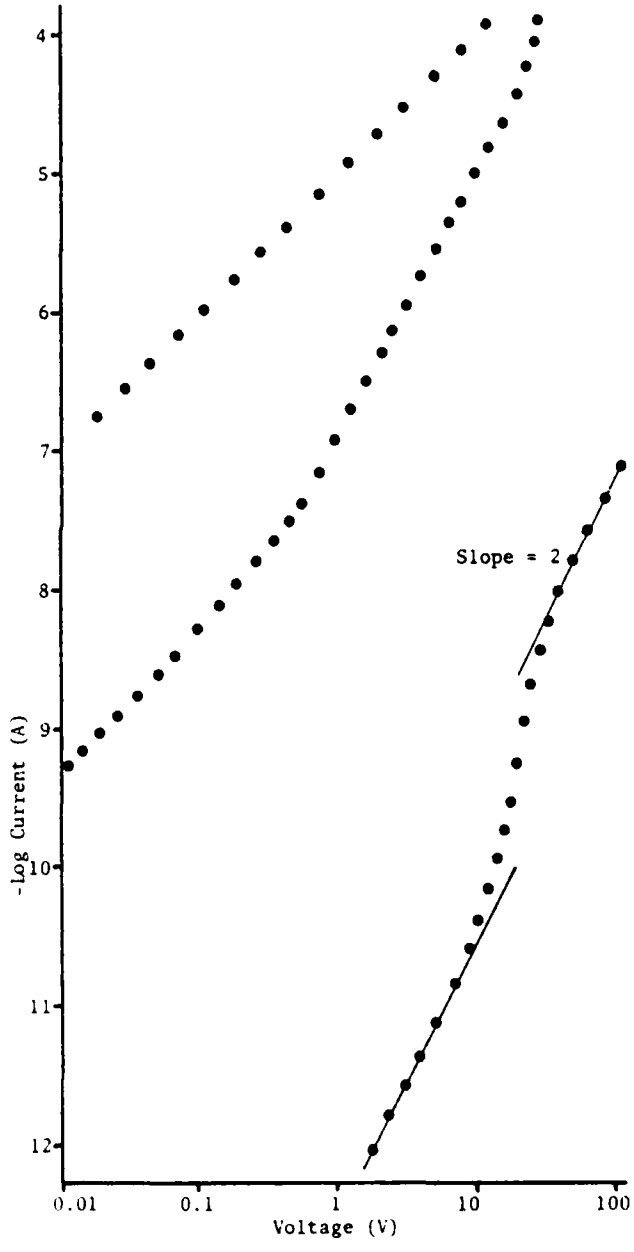

Figure 2. I-V curves for degraded 10nF devices.

A common characteristic seen in conjunction with SCLC is hysteresis, as shown in Figure 3, which is discussed further below.

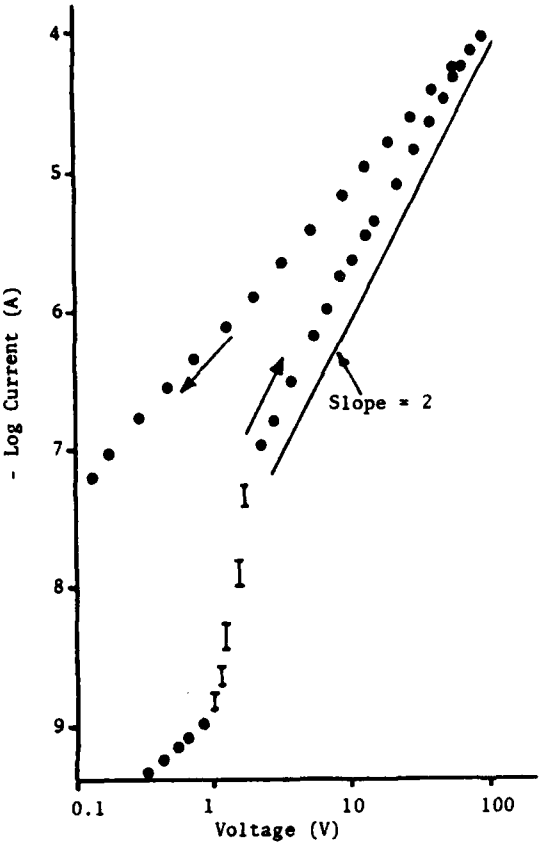

Figure 3. Hysteresis characteristic for degraded 10nF X7R device.

Activation energies for new X7R devices were measured to be 1.28 $\pm$ 0.03 eV. An example is shown in Figure 4.

It was found that activation energies were always less for degraded devices, i.e. as ceramic resistivity dropped so did activation energy. This dependence is shown in Figure 5 (using resistivity values at 125°C). Degraded devices with activation energies near zero have resistivities of about 10^5 Ωcm or less, and are ohmic. For 10nF devices, with area to thickness ratio of about 60, this corresponds to leakage resistance of roughly 2 KΩ or less.

The 3/2 or near -3/2 power dependence seen for new devices is not easy to fit to a planar electrode SCLC model, since due to trap filling, the voltage exponents are generally two or greater. (A point emission model that predicts 3/2 power behavior is discussed below).

Current Types

Neither Schottky nor Poole-Frenkel types of currents were identified. Even though a near-linear ℓn I vs. $V^{1/2}$ characteristic was occasionally obtained over a certain range of voltages, the slope of the curve was much too large to be attributed to Schottky or Poole-Frenkel emission. As determined from equation 6, assuming a dielectric constant of 2000 and electrode spacing of 6×10^{-5} m, a Poole-Frenkel slope of about

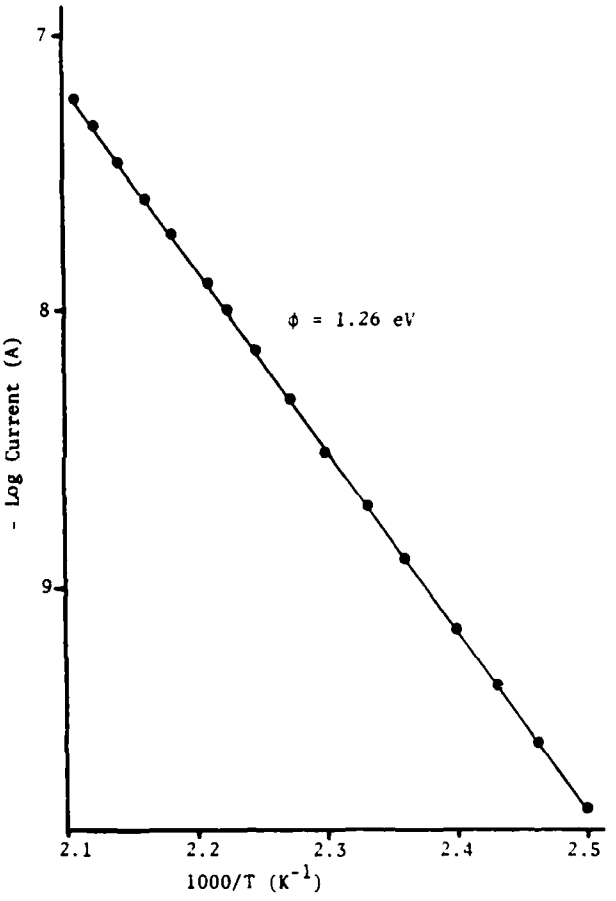

Figure 4. Arrhenius plot for new X7R device.

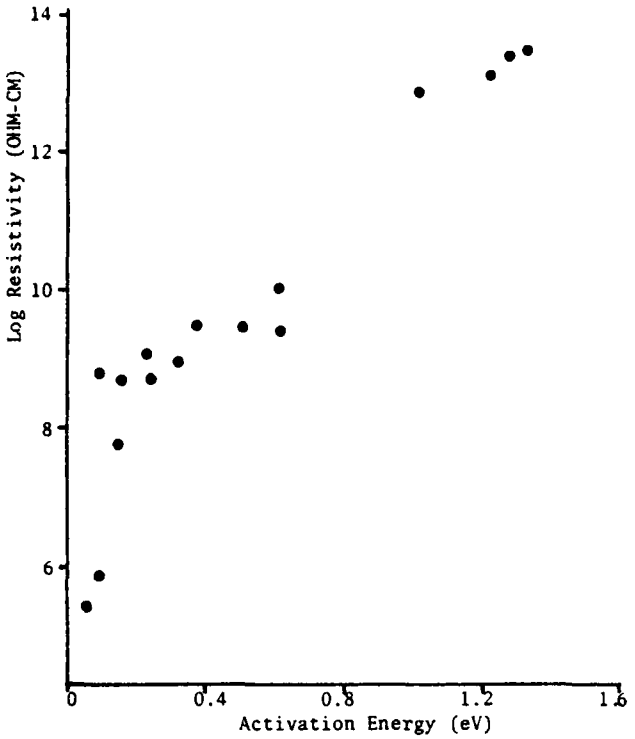

Figure 5. Dependence of resistivity on activation energy for X7R devices.

10^{-5} $(m/V)^{1/2}$ results, whereas experimental values are closer to 10^{-2} $(m/V)^{1/2}$. If one assumes a dielectric constant of only 10, a slope of about 10^{-3} $(m/V)^{1/2}$ results, which is still too small by an order of magnitude. In addition, since capacitance values remain essentially unchanged even for quite severely degraded devices, there is no indication that the dielectric constant is altered over a substantial volume of the capacitor.

What is the charge carrier? For all degraded devices (where a power law higher than 3/2 is followed) the SCL and ohmic currents are best described by electron flow. Thermoelectric coefficients for X7R chips with no internal electrodes are negative, indicating n-type behavior. Since the charge carriers for SCLC originate at the electrodes, ionic carriers can be ruled out.

For the undegraded capacitor also, a case can be made that the electron is the main carrier, under steady state conditions. Firstly, the 3/2 power model proposed below is based on electron emission, since it pertains to SCLC. Secondly, consider the leakage current exhibited by a 10nF X7R capacitor under lifetest at 180°, 800V. Its current remained steady at $\sim$ 0.5 μA for 5 days. If this current were due solely to doubly charged ion movement, it would result in over 10^{20} oxygen vacancies per cm^3. It is unlikely that the current could remain constant as such a large oxygen vacancy concentration developed. A more likely state is that electron flow predominates, accompanied by a smaller, ultimately degrading ion current in the same direction.

Another characteristic of interest is the hysteresis seen in Figure 3, which may be indicative of trap filling. It was noticed that upon heating to $\sim$ 100°C following such a run, the characteristic had reverted back to the lower curve, perhaps due to the thermal emptying of traps. If the thermally stimulated current (TSC) is measured during such heating, immediately after the device has seen 100 volts, a substantial current peak (about -3 nA for a 10nF capacitor) is seen at $\sim$ 50°C, which does not occur if another heating cycle is followed immediately thereafter. Such a TSC behavior might indicate the emptying of traps that were filled on the previous I-V run. However, it was found that this TSC peak was essentially the same for new and degraded devices, indicating that it is probably largely a depolarization current.[24] More extensive and refined TSC measurements on degraded devices such as these might yield trap parameters such as energy, lifetime etc.

Modelling

A model has been devised related to the 3/2 or near -3/2 power behavior seen for new X7R devices. It is known that 3/2 power behavior can be used to describe electron emission into a solid from a hemispherical electrode, an example for shallow traps being given in equation (5). Electron emission from electrode protuberances could result in a $V^{3/2}$ current dependence for MLC capacitors. Then one must ask why the 3/2 dependence transforms into a higher power (quadratic being common) as the device degrades.

Consider an electrode model where conductor protuberances occur due to the existence of ceramic pores, grain boundaries etc. in the electrode region (Figure 6).

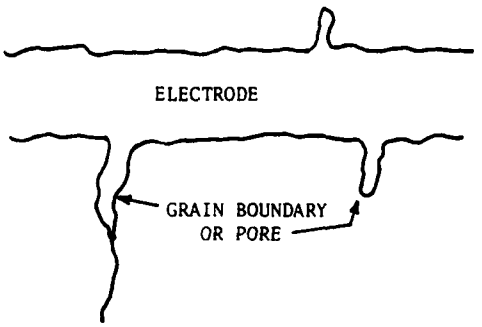

Figure 6. Electrode protuberances which can preferentially emit electrons.

Processes near the electrodes that could change the current from a 3/2 power SCLC behavior to quadratic (αV^2) as degradation occurs might be as follows: Initially, 3/2 power current from the cathode protuberance dominates. The field adjacent to the tip will be much larger than at the more planar cathode region. Oxygen ions will diffuse away from the tip preferentially, and a lower resistivity region will thus spread outward from the tip. The effective tip radius is thus increased due to the reduction of the field in the reduced resistivity region, and 3/2 power emission becomes less predominant. For more severe degradation, such effects could be so pronounced that tip emission would be more or less nullified, and the electrodes would appear (as far as electron emission is concerned) nearly planar. A simultaneous increase in oxygen vacancy and conduction electron densities in the ceramic body results in overall resistivity decrease

and current increase. Hence the transformation from a 3/2 power to square low voltage dependence, with simultaneous increase in leakage current.

Even an order of magnitude estimate of the current emitted from such a point or network of points is at present difficult, because most of the key parameters are unknown, including density of points, carrier mobility and concentration, trap parameters, etc., in the ceramic adjacent to the emitter.

This model is therefore somewhat speculative, but does predict the observed voltage behavior. Other models are of course available, such as field dependent ion-flow[18], and field dependent electron mobility[19,22], but these are even more speculative since the voltage dependence is arrived at indirectly by means of field dependent charge transport.

For the degraded MLC X7Rs that we have measured, the quadratic or near quadratic voltage behavior is the most common type seen. What information can be obtained from such a characteristic? Consider the generic SCLC characteristic shown in Figure 7, for the case of shallow traps.

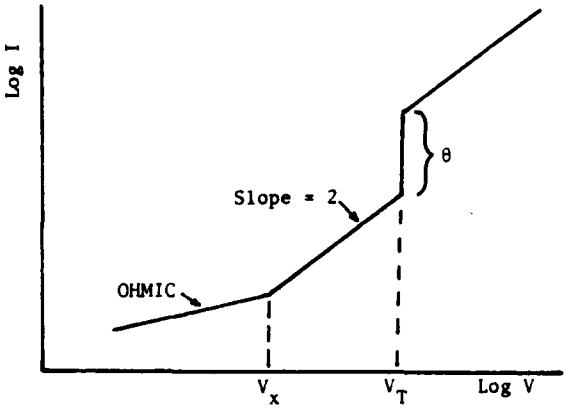

Figure 7. Generic ohmic-SCLC characteristic for degraded device.

Estimates can be made of certain parameters, under the assumption that the steep characteristic is due to shallow trap filling as more electrons are injected from the contacts. If trap filling occurs at voltage V_T, then equation (3) can be solved for mobility. One obtains

$$\mu \approx \frac{I L^3}{A\theta\epsilon V_T^2} \qquad (7)$$

The trap density can be estimated from the relation[16]

$$N_t \approx \frac{10^6 K V_T}{L^2} \qquad (8)$$

where K is the dielectric constant and other parameters were defined previously. The trap distance, in energy, from the conduction band edge can be expressed (using equation 4)

$$\Delta E = kT \ln \frac{N_c}{2\theta N_t} \qquad (9)$$

We have used the following parameters related to 10nF X7R devices that show SCLC trap filling such as that seen in Figure 2: $A = 0.36\ cm^2$, $L = 0.006$ cm, $\epsilon = 1.8\times10^{-10}$ F/cm.

The following ranges were obtained:

mobility: $10^{-7} < \mu < 10^{-2}\ cm^2/Vsec$

trap concentration: $10^{14} < N_t < 10^{15}\ cm^{-3}$

trap location: $0.4 < E_t < 0.6$ eV

The large mobility range results from equation (7) due to the large increase in I seen as devices degrade, with V_T remaining relatively constant, in the 1-10 V range. This is consistent with the fact that the ohmic and SCL quadratic currents both increase as a device degrades, each being proportional to mobility. In this regard, it should be noted that if only the carrier concentration increased during degradation (and if mobility remained constant), then only the ohmic part of the curve would increase in current; V_x in Figure 7 would increase, and the SCL current would be unchanged for $V > V_x$. This is because the SCL current does not depend on the background carrier concentration in the ceramic, but on emission from the electrodes, and, for transport, mobility. This implies for these devices, that a mobility increase may be just as significant a contributor to leakage current as the carrier concentration increase, during degradation. Mechanisms for such a mobility increase are at present not known, but may include grain boundary barrier height reduction (due to charge accumulation), hopping potential decrease, or other factors, depending on what actually controls the mobility. One indicator of a reduction in transport potential barriers (two examples mentioned above) could be the decrease in current activation energy ϕ, as shown in Figure 5. In equation (2), ϕ can be represented as $\phi = \phi_c + \phi_m$, where ϕ_c and ϕ_m are carrier concentration and mobility activation energies respectively. Since equation (2) is followed experimentally, we anticipate that carrier concentration and mobility might follow similar relations, firstly because of the large changes in μ noted above, and secondly because this is what was conclusively demonstrated by Nagels for $LiNbO_3$[25]. He reported electron conduction by means of small polarons, with both carrier concentration and mobility varying exponentially with temperature. Whether or not this is the case for X7R ceramic is being investigated by us by means of thermal emf and conductivity, and will be reported in a separate communication.

V. Conclusions

1. Steady state DC leakage currents for X7R MLC capacitors are ohmic at low voltages; at higher voltages follow a near-$V^{3/2}$ dependence when new, evolve into a V^2 behavior during degradation, and subsequently, with further degradation, become ohmic over the entire voltage range of the device;

2. The 3/2 and quadratic voltage behavior can be modelled after space charge limited currents; the 3/2 case attributed to electron emission from cathode points, the quadratic case to emission from planar electrode regions;

3. Electrons appear to be the dominant charge carrier, with thermoelectric polarity on X7R chips indicating n-type behavior;

4. Schottky or Poole-Frenkel currents were not identified;

5. Thermal activation energies decrease from $\sim$ 1.3 eV to zero as resistivity (at 125°C) decreases from $\sim 10^{13}$ Ω-cm to $\sim 10^{5}$ Ω-cm or less;

6. Estimates of drift mobility, trap concentration and trap energy ranges were made from quadratic SCLC characteristics;

7. It is possible that mobility increase, (in addition to carrier concentration increase), plays a dominant role in leakage current increase during degradation.

Acknowledgements

We would like to acknowledge the Office of Naval Research (Dr. Robert C. Pohanka) for supporting this research. We would also like to acknowledge Corning Electronics for providing capacitors and capacitor chips, and Dr. Neal Kenny of Corning for many helpful discussions.

References

[1] William J. Minford, "Accelerated Life Testing and Reliability of High K Multilayer Ceramic Capacitors", IEEE Trans. Components, Hybrids and Manuf. Technol., CHMT-5, 297 (1982).

[2] "The Reliability of Multilayer Ceramic Capacitors", Publication NMAB-400, National Academy of Sciences, Washington, DC (1983).

[3] Eugene Loh, "A Model of DC Leakage in Ceramic Capacitors", J. Appl. Phys. 53, 6229 (1982).

[4] C. Schaffrin, "Oxygen Diffusion in $BaTiO_3$ Ceramic", Phys. Stat. Sol. (a), 35, 79 (1976).

[5] R. Stumpe, D. Wagner and D. Bauerle, "Influence of Bulk and Interface Properties on the Electric Transport in ABO_3 Perovskites", Phys. Stat. Sol. (a) 75, 143 (1983).

[6] S. A. Long and R. N. Blumenthal, "Ti-Rich Nonstoichiometric $BaTiO_3$: I, High-Temperature Electrical Conductivity Measurements", J. Amer. Ceram. Soc. 54, 515 (1971).

[7] N. H. Chan, R. K. Sharma and D. M. Smyth, "Nonstoichiometry in Acceptor-Doped $BaTiO_3$", J. Amer. Ceram. Soc. 65, 167 (1982).

[8] Jeffrey D. Keck, "Electrical Degradation in High Purity Barium Titanate", Ph.D. Thesis, Univ. of Missouri-Rolla, 1976.

[9] L. Benguigi, "Electrical Phenomena in Barium Titanate Ceramics", J. Phys. Chem. Sol. 34, 573 (1973).

[10] W. A. Schultze, L. E. Cross, and W. R. Buessem, "Degradation of $BaTiO_3$ Ceramic Under High ac Electric Field", J. Amer. Ceram. Soc. 63, 83 (1980).

[11] Y. Y. Sabara, A. Y. Kudzin and K. A. Kolesnichenko, "Space Charge Limited Currents in Barium Titanate Single Crystals", Phys. Stat. Sol. (a) 38, K131 (1976).

[12] L. Benguigi, "Space Charge Limited Currents in $BaTiO_3$ Single Crystals", Sol. St. Commun. 7, 1245 (1969).

[13] R. T. Thomas, "Time Dependence of the Electrical Conductivity of $BaTiO_3$ Single Crystals Heated in Oxygen", J. Phys. D: Appl. Phys., 3, 1434 (1970).

[14] D. D. Glower and R. C. Heckman, "Conduction-Ionic or Electronic-in $BaTiO_3$", J. Chem. Phys. 41, 877 (1964).

[15] D. L. Ridpath and D. A. Wright, "Electrical Conductivity of Reduced Barium Titanate Crystals", J. Mater. Sci. 5, 487 (1970).

[16] M. A. Lampert and P. Mark, Current Injection in Solids, Academic Press (1970).

[17] M. A. Lampert and R. B. Schilling, "Current Injection in Solids: The Regional Approximation Method"; Ch. 1 in Semiconductors and Semimetals, Vol. 6 (ed. by R. K. Willardson and A. C. Beer), Academic Press (1970).

[18] J. J. O'Dwyer, The Theory of Electrical Conduction and Breakdown in Solid Dielectrics, Clarendon Press (1973).

[19] B. C. Eu and A. S. Wagh, "Nonlinear Field Dependence of Carrier Mobilities and Irreversible Thermodynamics in Semiconductors", Phys. Rev. B. 27, 1037 (1983).

[20] J. B. Gunn, "Instabilities of Current in III-V Semiconductors", IBM Jour. 141 (April 1964).

[21] K. Biedrzycki, K. Sujak-Lesz and J. Lesz, "Production of Free Charge Carriers (Exoelectrons) Over the Surface of Powdered Ceramics (Ba,Ti) TiO_3 5% Pb", Acta Physica Polonika A47, 801 (1975).

[22] S. M. Sze, Physics of Semiconductor Devices (2nd Ed.), John Wiley and Sons (1981).

[23] J. Burnham and E. Wong, "Failure Mechanism on Accelerated AC Test for High Voltage Capacitors", IEEE Reliability Physics Symposium Proceedings, p. 223 (1974).

[24] P. Braunlich (ed.), Thermally Stimulated Relaxation in Solids, Springer-Verlag (1979).

[25] P. Nagels, "Experimental Hall Effect Data for a Small-Polaron Semiconductor", from The Hall Effect and Its Applications (C. L. Chien and C. R. Westgate, ed.), Plenum Press (1980).

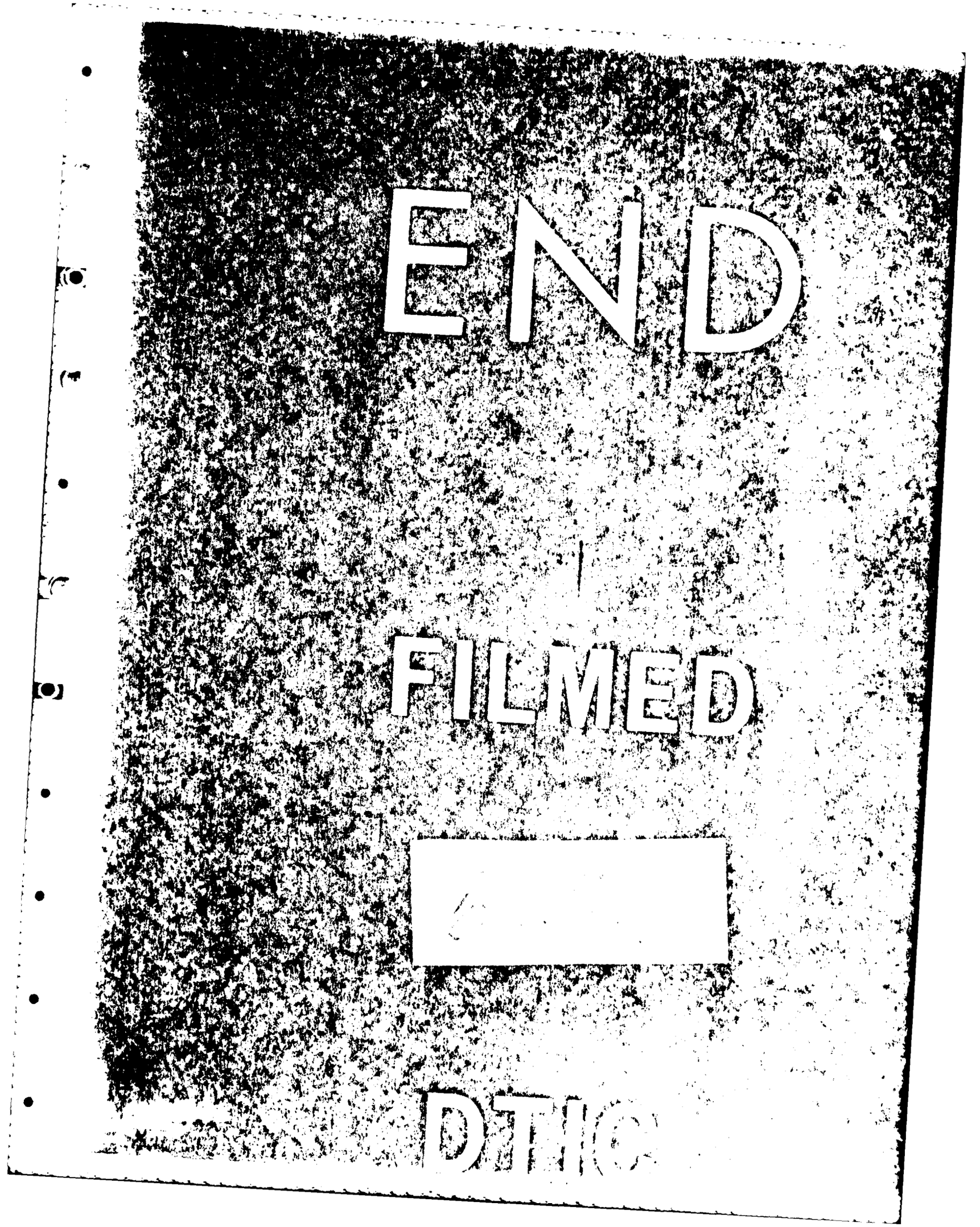
END
FILMED
DTIC